Formation of Widmanstätten Ferrite at Very High Temperatures in the Austenite Phase Field

Rupanjit Kaur Grewal

Supervisors: Professor John J. Jonas, Professor Stephen Yue

Department of Mining and Materials Engineering
McGill University, Montreal
November 2015

A thesis submitted to McGill University in partial fulfillment of the requirements of the degree of Masters of Engineering

Abstract

The present study was carried out on a Gleeble 3800 thermomechanical system. Compression tests were performed on a 0.06wt%C-0.3wt%Mn-0.01wt%Si steel over the test temperature range from 1000 to 1350 ºC (at 50º intervals). The deformed samples were water quenched. The samples were then polished, etched and examined using optical microscopy and EBSD techniques. The optical micrographs revealed the presence of plates of Widmanstätten ferrite at all test temperatures. The volume fractions of ferrite formed were measured and found to increase with temperature. This trend is shown to be consistent with the shape of the free energy obstacle calculated using the FactSage thermodynamic software. The dynamic transformation critical strains were determined using the double differentiation method. These were again consistent with the obstacle shape. Vickers microhardness measurements also supported the above interpretation. The high magnification EBSD micrographs indicated that the self-accommodating plates formed at high temperatures were about an order of magnitude wider than the plates formed below 1000 ºC. The results of the present study have revealed that the well-known Fe-C binary phase diagram is not applicable to austenite being deformed above the Ae_3 temperature. A possible 'metastable' phase diagram is proposed for use under dynamic conditions.

Résumé

La présente étude a été effectuée à l'aide d'un système thermomécanique Gleeble 3800. Des tests de compression ont été faits sur un acier 0.06wt%C-0.3wt%Mn-0.01wt%Si à des températures allant de 1000 à 1350 ºC (à 50º d'intervalle). Les échantillons déformés ont été trempés à l'eau. Ces échantillons ont ensuite été polis, soumis à une attaque chimique, et examinés à l'aide de la microscopie optique et des techniques EBSD. Les micrographes optiques ont révélés la présence de plaques de ferrite Widmanstätten à toutes les températures testées. Les fractions volumiques de ferrite ont été mesurées et il a été observé que ces volumes augmentent de pair avec la température. Cette tendance est consistante avec la courbe d'obstacle d'énergie libre calculée en utilisant le logiciel FactSage. Les tractions critiques de transformation dynamique ont été déterminées à l'aide de la méthode de différentiation double. Celles-ci ont été encore une fois consistantes avec la courbe d'obstacle d'énergie. Les mesures Vickers de microdureté supportent aussi l'interprétation mentionnée ci-haut. Les micrographes EBSD à haute magnification ont indiqué que les plaques auto-accommodantes formées à de hautes températures étaient un ordre de magnitudes plus larges que les plaques formées sous 1000 ºC. Les résultats de la présente étude ont révélés que le diagramme de phase binaire Fe-C déjà bien connu n'est pas applicable à l'austénite qui est déformée au-dessus de la température Ae_3. Un diagramme de phase 'métastable' possible est proposé lorsque des conditions dynamiques sont présentes.

Contributions of the Authors

This thesis was prepared according to the guidelines published by the Graduate and Postdoctoral Studies office of McGill University for a manuscript-based thesis. The present document is based on the following manuscript:

Rupanjit Grewal, Clodualdo Aranas Jr., Kanwal Chadha, Davood Shahriari, Mohammad Jahazi, John J. Jonas, “Formation of Widmanstätten ferrite at very high temperatures in the austenite phase field,” submitted to Acta Materialia, Ms. No. A-15-2601.

The manuscript was co-authored with my supervisor, Prof. John J. Jonas. My colleague Clodualdo Aranas Jr., helped and trained me on using compression equipment and carrying out computer simulations. Prof. Mohammad Jahazi and his team, Davood Shahriari and Kanwal Chadha, of the École de Technologie Supérieure, assisted me in performing the compression tests on their Gleeble 3800 system.

Acknowledgements

The success of any project depends largely on the encouragement of many other people. I take this opportunity to express my gratitude to those who have been instrumental in the successful completion of this thesis.

Firstly, I would like to thank my supervisor Professor John J. Jonas for his guidance, enthusiasm and persistent help during the course of my research. I would also like to acknowledge my co-supervisor Professor Stephen Yue for his valuable assistance.

I express my special gratitude to Professor Mohammed Jahazi and his team at the École de Technologie Supérieure for their assistance during the experimentation. I am also thankful to my colleague and good friend Clodualdo Aranas Jr. for his most helpful advice, which led to the successful completion of my work.

Contents

List of figures

List of Tables

Chapter 1: Introduction

1.1 Introduction

The dynamic transformation of austenite to ferrite was first studied by Yada and coworkers in the 1980's [1]. They employed compression tests and rolling simulations and showed that ferrite can be formed in the fully austenitic zone at temperatures as high as 160 ºC above the Ae_3 line. Little follow-up work was done for the next decade. Then, Yada and coworkers returned to the topic of dynamic transformation in 2000, where they confirmed the occurrence of the phase transformation in a real time system by using in-situ X-ray examination while simultaneously running the torsion tests [2]. Chen and Chen in 2003 showed that the reverse transformation of ferrite to austenite occurs when the samples are held at temperature after deformation [3]. Various researchers have discussed different aspects of this softening phenomenon [4-7].

More recently, Ghosh *et al*. in their study of 2013 proposed a model that included both the forward as well as the reverse transformation [8-10]. They introduced the concept of mechanical activation that could account for the displacive forward transformation. Still more recently, Aranas *et al.* [11, 12] proposed that the driving force required for dynamic phase transformation is the difference in the flow stress of the strain hardened austenite and the yield stress of ferrite that takes its place. This research also suggested that it should be possible to produce dynamic transformation at very high temperatures in the austenite phase field.

The aim of the present study was, therefore, to investigate the possible formation of Widmanstätten ferrite at very high temperatures in the austenite phase field. This

subject is treated as follows. In **Chapter 2**, recent progress in the field of the dynamic transformation of austenite is reviewed. In **Chapter 3**, the results of the present investigation are described in detail in the form of a paper that has been submitted for publication. Finally, the entire study is summarized in the concluding **Chapter 4**. There is also an appendix in which an improved diagram is shown, which is intended for insertion into the published paper.

1.2 References

1. Y. Matsumura, H. Yada, Evolution Deformation of Ultrafine- Grained Ferrite in Hot Successive Deformation, Transactions ISIJ. 27 (1987), 492-498.
2. H. Yada, T. Matsumura, T. Senuma, Proc. Int. Conf. Physical Metallurgy of Thermomechanical Processing of Steels and Other Metals, ISIJ, THERMEC 88, (1988) 200-207.
3. H. Yada, C.M. Li, H. Yamagata, Dynamic γ→α Transformation during Hot Deformation in Iron-Nickel-Carbon Alloys, ISIJ international. 40 (2000), 200-206.
4. Y. Chen, Q. Chen, Dilatometric Investigation on Isothermal Transformation after Hot Deformation, J. Iron & Steel Res. Int. 10 (2003) 46-48.
5. H. Dong, X. Sun, Deformation Induced Ferrite Transformation in Low Carbon Steels, Current Opinion in Solid State Mater. Sci. 9 (2005) 269-276.
6. M. Tong, J. Ni, Y. Zhang, D. Li, Y. Li, Monte Carlo-Method Simulation of the Deformation-Induced Ferrite Transformation in the C-Fe system, Metallurgical and Materials Transactions A. 35A (2004) 1565-1577.
7. N. Park, A. Shibata, D. Terada, N. Tsuji, Flow Stress Analysis for Determining the Critical Condition of Dynamic Ferrite Transformation in 6Ni-0.1C Steel, Acta Mater. 61 (2013) 163-173.
8. C. Ghosh, V.V. Basabe, J.J. Jonas, Y-M. Kim, I-H. Jung, S. Yue, the Dynamic Transformation of Deformed Austenite at Temperatures above the Ae_3, Acta Materialia. 61 (2013) 2348-2362.

9. C. Ghosh, V.V. Basabe, J.J. Jonas, Thermodynamics of Dynamic Transformation of Hot Deformed Austenite in Four Steels of Increasing Carbon Content, Material Science & Engineering A. 591 (2014) 173 -182.

10. J.J. Jonas, C. Ghosh, Role of Mechanical Activation in the Dynamic Transformation of Austenite, Acta Materialia. 61 (2013) 6125-6131.

11. C. Aranas, J.J. Jonas, Effect of Mn and Si on Dynamic Transformation of Austenite Above the Ae_3 Temperature, Acta Materialia. 82 (2015) 1-10.

12. C. Aranas, T. Nguyen-Minh, R. Grewal, J.J. Jonas, Flow Softening-based Formation of Widmanstätten Ferrite in a 0.06%C Steel Deformed Above the Ae_3, ISIJ International. 55 (2015) 300-307.

Chapter 2: Literature Review

In this chapter, the various phases present in conventional iron-carbon phase diagrams are described. The literature review then surveys the softening mechanisms associated with dynamic recrystallization and dynamic transformation. This covers the pioneering works of the 1980's and continues to the latest developments of the past few years. The review then leads to the main objectives of this study.

2.1 Iron-Carbon Phase Diagram

In the iron-carbon equilibrium phase diagram (**Fig. 2.1**), the composition of carbon is plotted against temperature. Pure iron undergoes a change in its crystal structure upon heating. Carbon acts as an interstitial impurity in iron. Its solubility differs at different temperatures and in the different phases of steel. In α-ferrite, the solubility of carbon in iron is only 0.008 wt.% at room temperature. Upon increasing the temperature (that is going up to 727 ºC) the carbon solubility increases to 0.022 wt.% in ferrite. The α-ferrite has a body centered cubic structure resulting in the limited solubility of carbon in iron. However, γ-ferrite has a face centered cubic structure and the solubility of carbon can go as high as 2.14 wt.% at 1147 ºC which is referred to as the eutectic point. This region, also known as austenite, is stable between 727 ºC and 1493 ºC. The δ-ferrite, which is crystallographically identical to α-ferrite, exists from 1394 ºC up till the melting point of iron, 1538 ºC. On cooling down from 1493 ºC at 0.15 wt.% carbon the δ-iron experiences a transformation completely into austenite. This point is called the peritectic point. Also, at a carbon composition of 0.76 wt.%, austenite cooled down from 727 ºC is transformed completely into α-iron and cementite. This is called the eutectoid point and

the boundary line is called the Ae_3 line. As the carbon content increases, the cementite (Fe_3C) phase is formed. This phase is brittle and very hard.

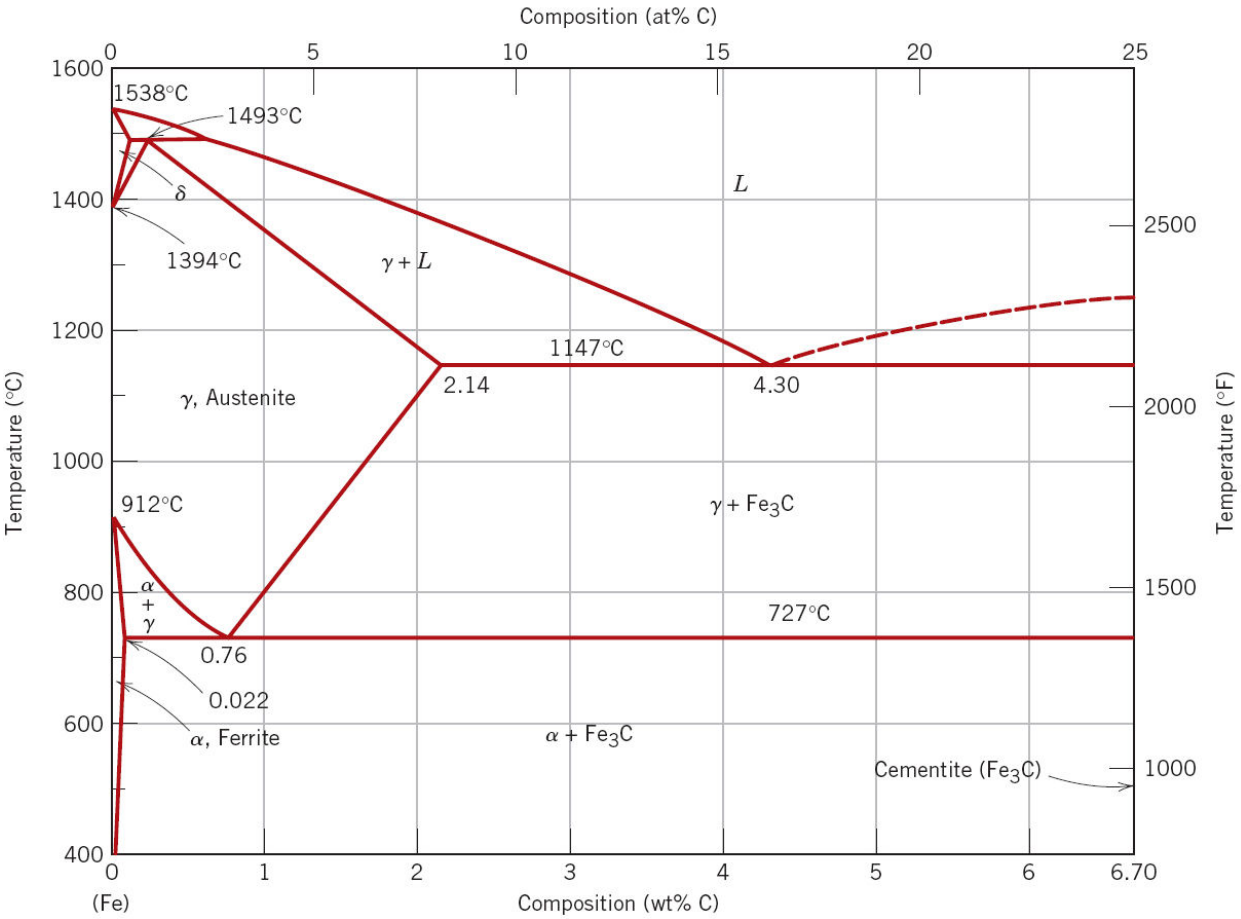

Fig. 2.1 The iron-carbon phase diagram, showing the equilibrium phases of carbon and iron with changing carbon concentration and temperature [1].

Ferrous alloys, that is, iron-based alloys, are extensively used in a wide range of industries. Depending upon the carbon content, these alloys can be broadly classified into two groups, namely, steel and cast iron. Apart from the reactions taking place in the binary iron-carbon system, the properties of steels can be conspicuously changed by the alloying elements added. For instance, austenite stabilizers are used to widen the temperature range of austenite formation and ferrite stabilizers, on the other hand, are

used to restrict formation of the austenite phase. Some of the notable austenite stabilizers used in the steel industry, are nickel, manganese, and molybdenum. Chromium, vanadium, silicon, and tungsten are the ferrite formers.

2.2 Phase Transformations of Austenite

Authors W. A. Soffa and D. E. Laughlin (2014) [2] state that "*A phase transformation in a material system occurs when one or more of the phases in a system changes their state of aggregation, crystal structure, degree of order or composition resulting from a reconfiguration of the constituent particles (atoms, molecules, ions, electrons, etc.) comprising the phase.*" In case of the phases formed in the iron-carbon phase diagram, phase transformations can be broadly divided into two types: reconstructive and displacive transformations (**Fig. 2.2**).

2.2.1 Reconstructive Transformations

Reconstructive diffusional transformations, also called civilian transformations, require the bit by bit dismantling of the parent phase into the bit by bit construction of a new phase [2]. The γ -> α transformation generally occurs close to the Ae_3 temperatures because high temperatures provides easy mobility for diffusion to occur. Allotriomorphic ferrite and pearlite take shape by this process.

2.2.1.1 Allotriomorphic Ferrite

Some authors have classified the ferrite formed by diffusional mechanism into two main forms: allotriomorphic and idiomorphic ferrite. Unlike its outer shape, an allotriomorphic phase has a crystalline internal structure [4]. This type of formation takes place during cooling from higher temperatures. Here, ferrite/austenite grain boundaries replace a

large portion of the austenite/austenite boundaries. The morphology of allotriomorphic ferrite is defined by its boundary contours. By contrast, idiomorphic ferrite has an equiaxed morphology and is seen to be nucleated at heterogeneous sites in steel (**Fig. 2.3**) [5].

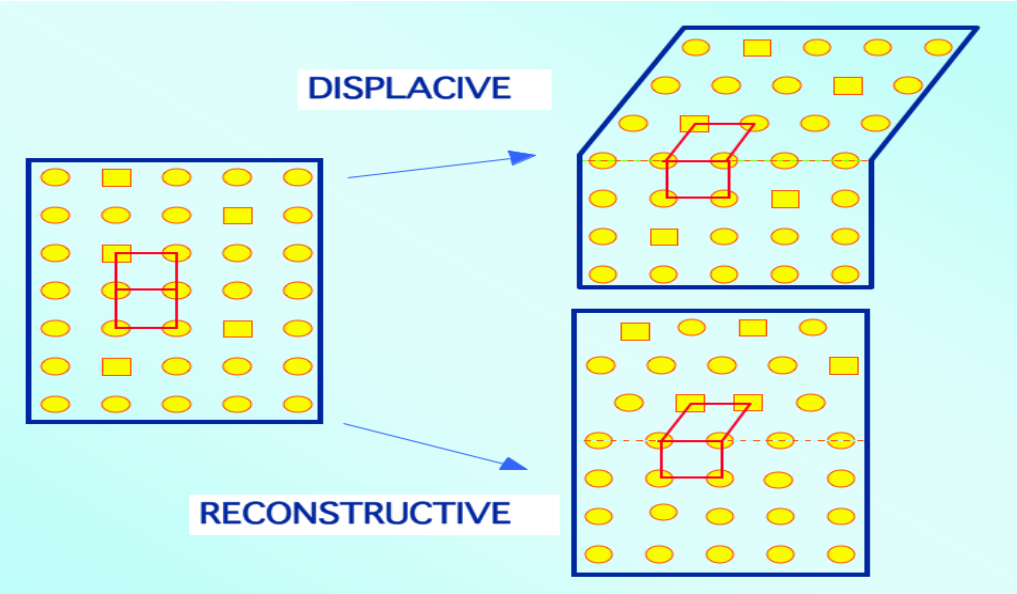

Fig. 2.2 Displacive and reconstructive mechanisms [3].

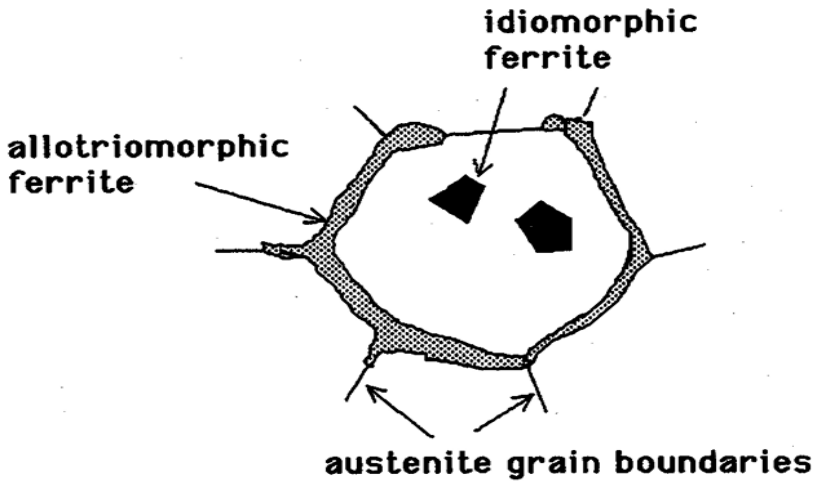

Fig. 2.3 Allotriomorphic and idiomorphic ferrite [3].

2.2.1.2 Pearlite

The lamellar structure of pearlite results from the diffusional and co-operative growth of cementite and ferrite within austenite cooled just below the lower critical temperature. This is known as the eutectoid reaction (**Fig. 2.1**). This reaction can be written as:

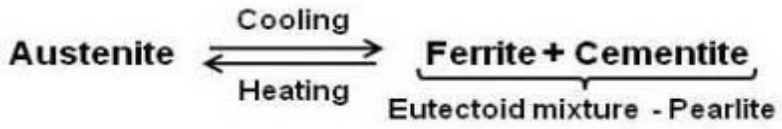

As discussed above, pearlite is constituted of alternate layers of cementite and ferrite. It is also important to mention that pearlite consists of 88% ferrite and 12% cementite. Another important feature to point out is that the ferrite formed here has a very low carbon content, which makes it almost pure iron whilst the other phase is cementite, which is 6.67 wt.% carbon. Therefore, it can be said that the pearlite transformation occurs by the diffusion of carbon atoms. Next, to determine which of the two nuclei was formed first, Mehl and his team [6] in 1956 introduced the following sequence of events. According to this model, a cementite platelet gets nucleated at the austenite grain boundary. Carbon from the austenite grain boundary then diffuses into this platelet. It increases the size of the cementite platelet. This, in turn, leads to a deficiency of carbon in the neighboring austenite which, thereupon, changes into ferrite. This results in the nucleation of ferrite around cementite platelets. This procedure can be seen in **Fig. 2.4**. **Fig. 2.5** shows the nucleation and growth of ferrite nodules in the surrounding austenite grains.

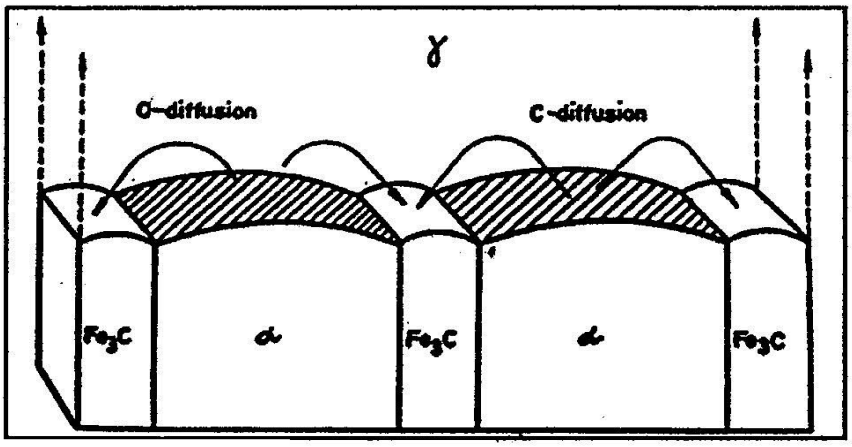

Fig. 2.4 Illustration of the formation and growth of pearlite [7].

2.2.2 Displacive Transformations

Displacive transformations, also known as military transformations, occur by means of the harmonized movement of atoms to form a new phase [2]. These transformations only affect the crystal structure as the atomic bonding remains unchanged. Displacive transformations are preferred during rapid cooling. Widmanstätten ferrite, bainite, and martensite are formed in this manner.

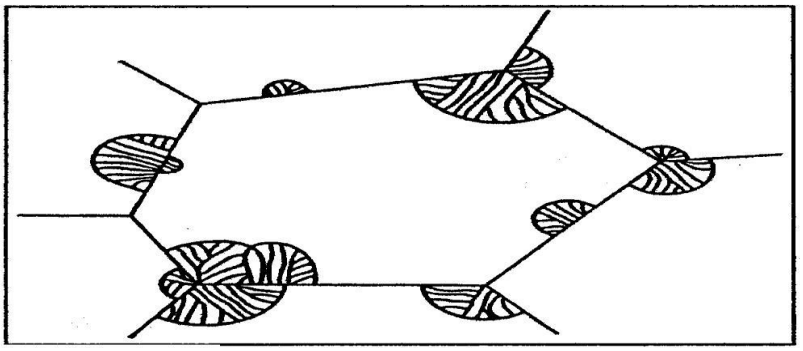

Fig. 2.5 Growth of pearlite nodules in the adjacent austenite grains [7].

2.2.2.1 Bainite

This mixture of ferrite and carbide is referred to as bainite. Bainite formation occurs over a wide temperature range. Mehl [8] established the two main categories of bainite as: upper bainite and lower bainite. These two types are formed over different temperature ranges and can be distinguished by their morphologies [9, 10]. A schematic representation of the formation of upper and lower bainite is shown in **Fig. 2.6**.

BF is the acronym used for bainitic ferrite, meaning the supersaturated ferrite component of bainite. Its upper limit is just below the minimum temperature required for pearlite formation and the lower limit being just above the beginning of martensite evolution. Growth of the plates occurs in clusters called sheaves. Upper bainite exhibits a feathery ferrite structure with carbide precipitation parallel to the needle axes. Each sheaf consists of parallel plates which have similar crystallography. This occurs over a temperature range of 550 to 400 ^{o}C. On the other hand, lower bainite displays an acicular ferrite structure in which the precipitated carbide is at an angle to the major axis of the plate. Here, the temperature range varies from 400 to 250 ^{o}C. Unlike upper bainite, cementite in lower bainite also precipitates in the ferrite (BF) plates and at the interphase grain boundaries giving it a particularly fine structure [11]. Due to its fine structure, bainite can only be studied under an electron microscope [12].

2.2.2.2 Martensite

The rapid quenching of austenite at room temperature results in the formation of yet another phase called martensite. In the transformation of austenite to pearlite and austenite to bainite, intense carbon diffusion occurs whilst in the case of martensite, no

carbon diffusion is observed. The reason for the latter is that martensite is formed below 200 ºC, by quenching, in a range where carbon diffusion takes place too slowly.

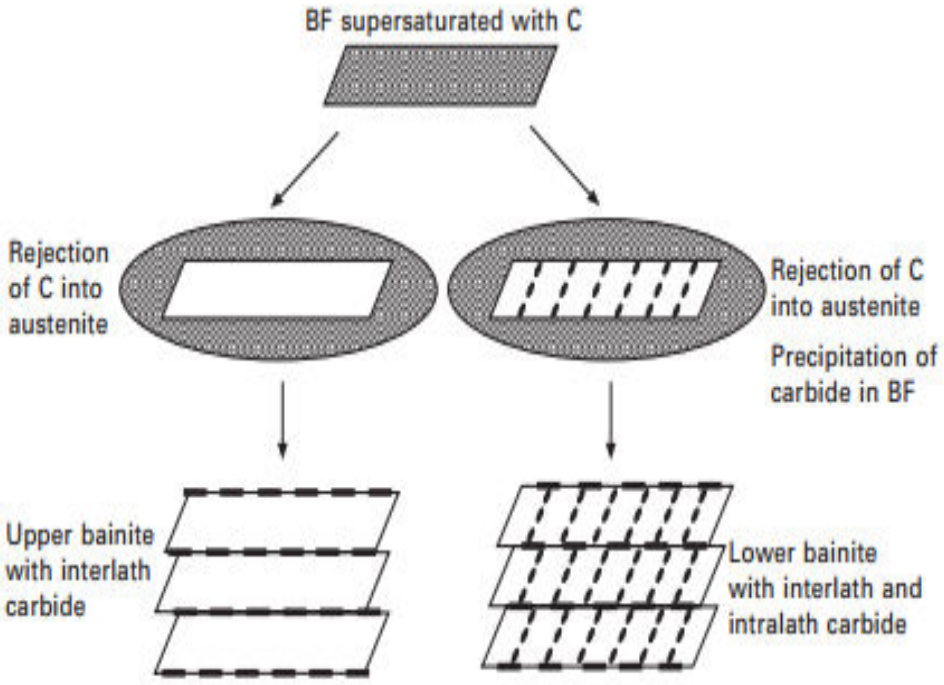

Fig. 2.6 Schematic portrayal of the upper bainite and lower bainite mechanisms [11].

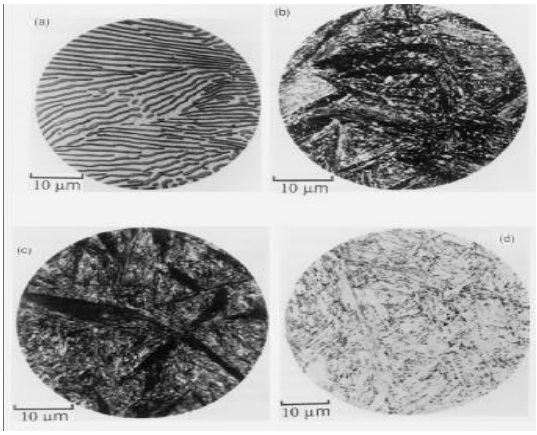

Fig. 2.7 Shows that in eutectoid steel (a) at 720 ºC: pearlite formation (b) at 290 ºC: bainite formation (c) at 180 ºC: bainite formation (d) at 180 ºC: martensite formation [13].

Fig. 2.8a shows two unit cells of austenite (grey circles) with carbon at their octahedral interstices (black circles). It is shown in the figure that these two unit cells are joined at their $(100)_F$ planes to comprise the body centered tetragonal structure of martensite (**Fig. 2.8b** and **Fig. 2.8c**). The BCT austenite, thus developed in **Fig. 2.8c** then contracts to form the BCT martensite [14].

Because the transformation is displacive, the formation and growth of martensite in a matrix takes place as swiftly as the velocity of sound. The microstructure of martensite is shown in the **Fig. 2.7** with comparison to pearlite and bainite. In general, the microstructure of martensite consists of plate-like planes and laths accompanied by the occasional emergence of rod-like laths [15].

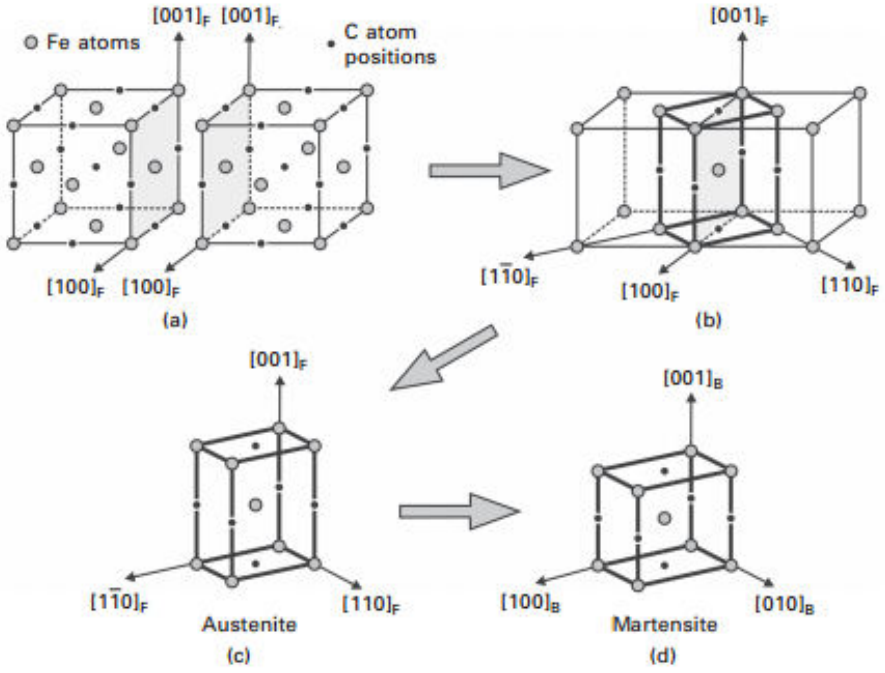

Fig. 2.8 The Bain model for martensite formation in steels [14].

2.2.2.3 Widmanstätten Ferrite

Widmanstätten ferrite is made up of long and pointed plates of ferrite which involve the simultaneous growth of pairs of plates (**Fig. 2.9**). It is chiefly classified into two forms: primary and secondary Widmanstätten ferrite. The former is said to nucleate along austenite grain boundaries and the latter along the ferrite/austenite grain boundaries.

Widmanstätten ferrite grows at high temperatures where the driving force is very small and the strain energy associated with single plates is high (600 $Jmol^{-1}$). This is impossible to sustain. So what happens is that, the Widmanstätten ferrite forms a pair of plates (instead of forming a single plate) (**Fig. 2.10**). In this way, the two plates tend to cancel out each other's strain energies. The strain energy is then reduced to 50 $Jmol^{-1}$. The aftermath of this formation mechanism is that these two α_w plates must nucleate at the same time, giving them a wedge shape [16].

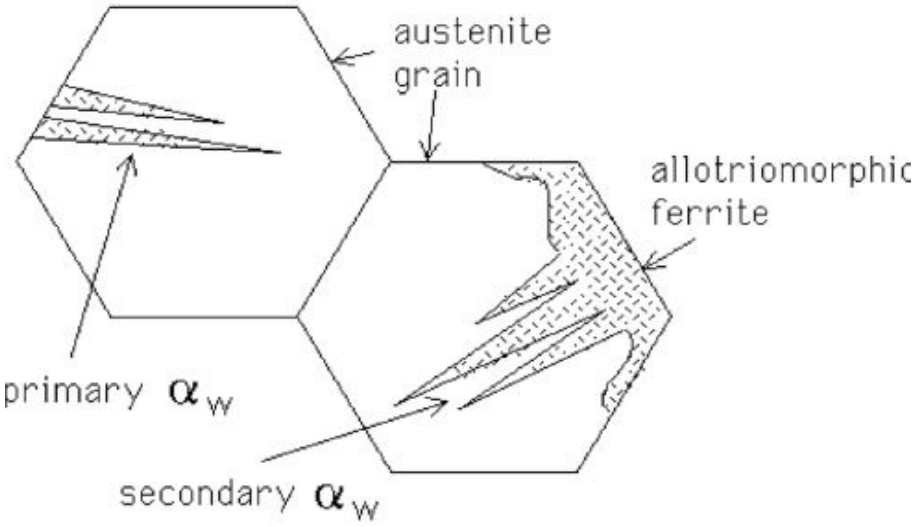

Fig. 2.9 Primary and secondary phases of Widmanstätten ferrite [16].

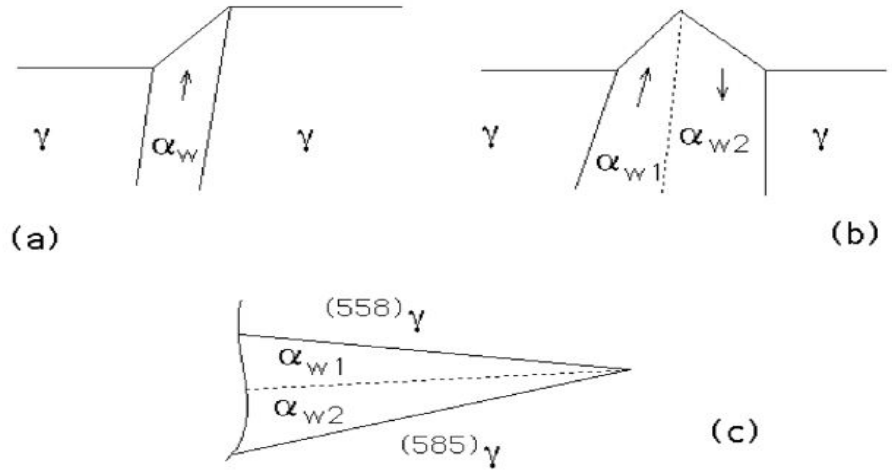

Fig. 2.10 Examples of the growth of two self-accommodating α_w plates [16].

As the phase transformation discussed here is displacive, Widmanstätten ferrite induces another feature known as paraequilibrium transformation. In paraequilibrium phase transformations, only the interstitial elements can diffuse quickly enough to reach equilibrium. Substitutional elements, such as, Mn, Cr, Si etc., are typically 'frozen in' during the transformation. So, growth in Widmanstätten ferrite is controlled by carbon diffusion ahead of the plate tip. **Fig. 2.9** shows the formation of primary and secondary Widmanstätten ferrite.

2.3 The Hot Rolling Process

In order to improve the mechanical properties of steel, such as, strength and toughness, rolling is one of the most beneficial processes. Rolling, which is also the dominant deformation process used in the world, is classified into two types: flat rolling and profile rolling. In flat rolling or strip rolling, the end product is in the form of a sheet whereas in profile rolling the final product generally has a non-planar cross section.

In hot rolling technology, the metal piece (or billet) is heated up to its austenization temperature, where the billet is fully austenitic. A typical rolling operation (**Fig. 2.11**)

consists of two types of mills: roughing and finishing mills. Roughing mills operate above the non-crystallization temperature (T_{nr}). In the roughing mill, the billet is plastically deformed while it is subjected to two constantly spinning rolls. The compressive forces exerted by the rolls lead to a decrease in the height of the billet. In this process, recrystallization prevails quickly, which gives rise to refinement of the austenite grains. On the contrary, finishing mills work just above and just below the austenite transformation temperature as well as the non-crystallization temperatures (T_{nr}). Typically, a finishing mill is made up of 7 mill stands. In this process, the austenite grains become elongated when recrystallization is incomplete. After this, the sheet enters into the high capacity coolers, where it is cooled by water jets. As a result of the cooling, the austenite transforms giving the steel sheet its final mechanical properties. Lastly, during the rolling process, both hardening and softening are observed. The deformation energy in the system is stored in the form of dislocations. The release of this energy takes place by two primary processes: recovery, and recrystallization.

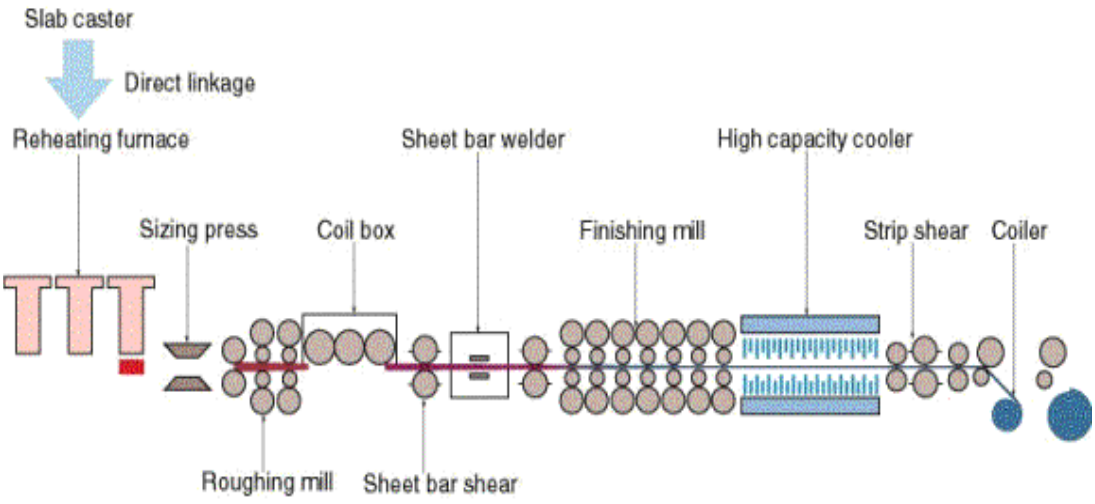

Fig. 2.11 Representation of a typical hot strip rolling mill [17].

2.3.1 Recovery

A generic definition of recovery was given by Doherty *et al.* in 1998 [18] as "*Recovery is all annealing processes occurring in deformed materials that occur without the migration of a high angle grain boundary.*"

Increasing temperatures, strains, and strain energies escalate the rate of recovery. As said in the definition above, there is no movement of high angle boundaries but the subgrain boundaries become sharp. In recovery, the repositioning of dislocations comes about to lower their lattice energies. Recovery is broadly classified into: static and dynamic recovery. The difference in the two is that, the latter takes place 'during' and the former occurs 'after' hot deformation processing.

2.3.2 Recrystallization

Recrystallization is the formation of new equiaxed and strain-free grains by the motion of high angle grain boundaries. Recrystallization can be sectioned into three categories: static, dynamic and metadynamic recrystallization.

2.3.2.1 Static Recrystallization

Static recrystallization (SRX), which is the most important softening mechanism, is found during the roughing interpass intervals and finishing intervals. Static recrystallization is strongly dependent on strain and temperature.

The behavior of SRX w.r.t strain and deformation temperature is shown in **Fig. 2.12**, as reported by Lin *et al*. in 2008 [19]. It can be seen that increasing the strain rate and deformation temperature affects the SRX notably. For static recrystallization to occur, minimum holding times are required and it is also necessary to reach a particular critical

strain value. It is also worth mentioning that alloying elements hinder the SRX process [20, 21].

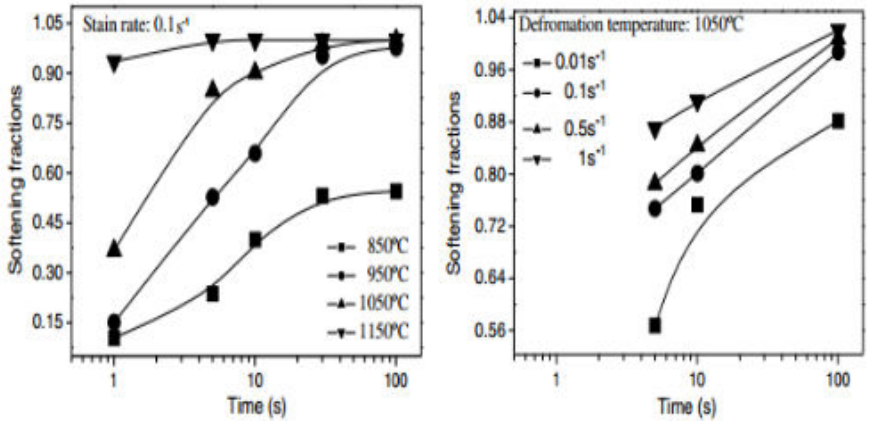

Fig. 2.12 Effect of deformation temperature and strain rate on SRX [19].

2.3.2.2 Dynamic Recrystallization

Dynamic recrystallization is an important softening mechanism in hot rolling because it promotes the refinement of austenite grains. This process occurs in the finishing passes in the strip rolling mill. DRX leads to mechanical properties in the end product which makes it desirable in many cases. For instance, when DRX occurs before austenite transformation and the sheet is cooled at the rate of 5 $^{o}Cs^{-1}$, ferrite grains less than 5 μm in diameter are observed [20].

2.3.2.3 Metadynamic Recrystallization

Metadynamic recrystallization (MDRX) is also one of the softening mechanisms that occurs during the unloading intervals. Though this effect is small it involves the growth of the DRX nuclei present at the end of the hot rolling process. MDRX has a high dependence on strain rate, unlike static recrystallization [22, 23].

Lin *et al*. (2009) [24] reported the effect of strain rate and deformation temperature on MDRX. In **Fig. 2.13**, it can be seen that at 30% deformation, the amount of MDRX softening increases with increasing temperatures. Concurrently, increasing the strain rate significantly affects the metadynamic softening behavior.

2.4 Dynamic Transformation of Austenite

In the pioneering work of Yada and coworkers in 1988 [25], they reported the formation of ultrafine ferrite above the Ae_3 temperature. It is important to discuss some of the remarkable results obtained by these authors.

In their hot deformation tests, they showed that “ultrafine” ferrite was in present in the martensite matrix when the deformed sample was quenched. As shown in **Fig. 2.14**, it can be seen that the amount of ferrite increased with strain but showed the opposite effects with temperature (1073 K and 1173 K). Calculation of the mean grain size (**Fig. 15**) also showed that the transformation of austenite took place while deforming the sample.

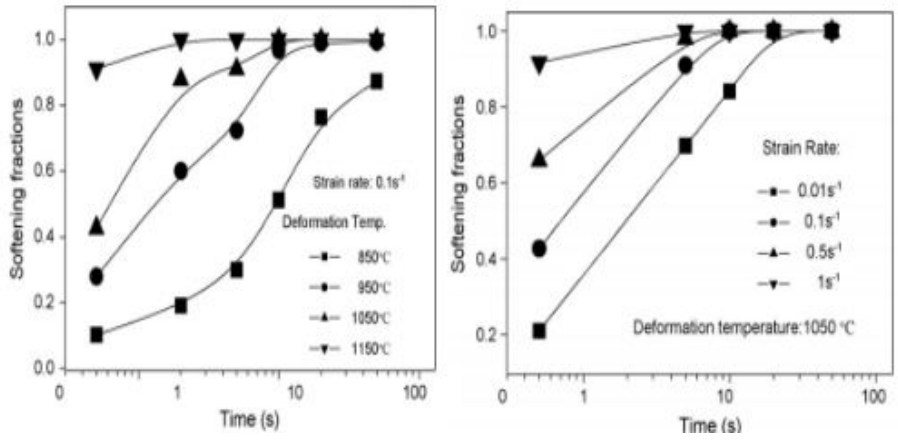

Fig. 2.13 Effect of deformation temperature and strain rate on MDRX [24].

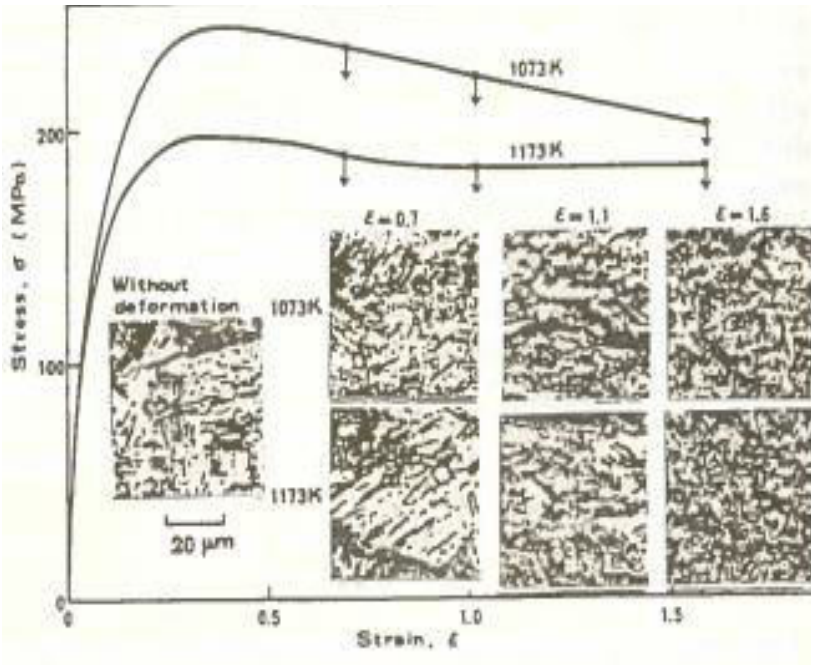

Fig. 2.14 Illustration of the effect of strain accompanied by the microstructural changes taking place [25].

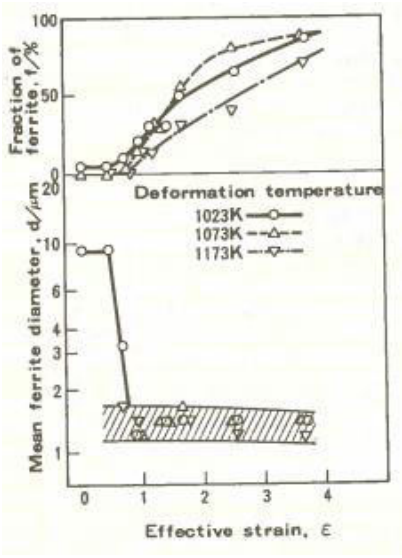

Fig. 2.15 Graphical representation of the volume fraction of ferrite formed w.r.t. deformation temperature and the mean grain size vs effective strain [25].

The authors also showed that if the deformed samples were held for increasing holding times, the ferrite became unstable and started vanishing. Also, upon testing the steel samples over a range of different interpass times, it was observed that ferrite remained unchanged for short interpass times (1s). The occurrence of dynamic recrystallization was also observed with increasing interpass time.

Yada and coworkers, in 2000 [26], performed an in-situ X-Ray real-time examination of low carbon samples deformed by torsion above the Ae_3 temperature. They used an in-situ X-Ray experimental set up to run alongside the torsion tests. The motive behind this experimentation was finding real-time evidence for the phase transformation. In **Fig. 2.16a)**, the diagram represents the specimen prior to heating, **b)** the next film witnesses the formation of austenite, which can be seen in the strong diffraction line $(111)_{\gamma\text{-Fe}}$ upon full austenization, and **c)** shows the development of another diffraction line $(110)_{\alpha\text{-Fe}}$ when the sample is subjected to deformation.

In their paper of 2003, Chen and Chen [27] demonstrated yet another breakthrough on the subject of dynamic transformation. On low carbon steel samples, they performed single pass and two pass deformations using a ThermecmasterZ simulator. They concluded that, during holding, the negative volume effect observed proved that the ferrite was undergoing a reverse transformation into austenite, as shown in **Fig. 2.17**. Another point worth mentioning here is that at 30 ^{o}C above the Ae_3 line, they showed that the forward transformation took place in fractions of a second but the reverse transformation took place in 45 s.

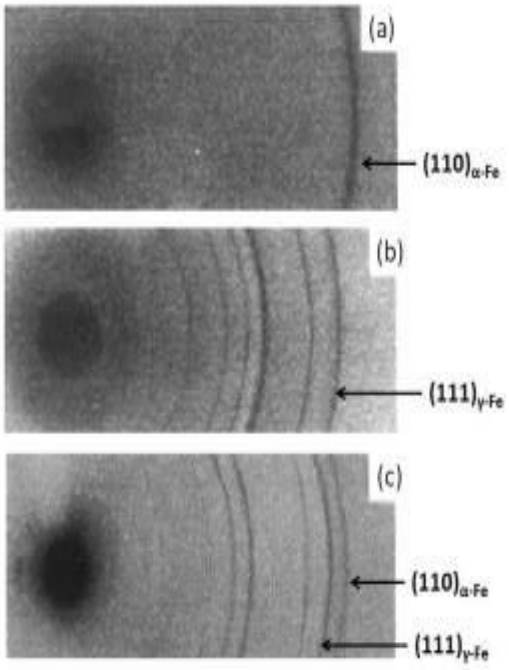

Fig. 2.16 X-ray diffraction patterns produced during torsion testing [26].

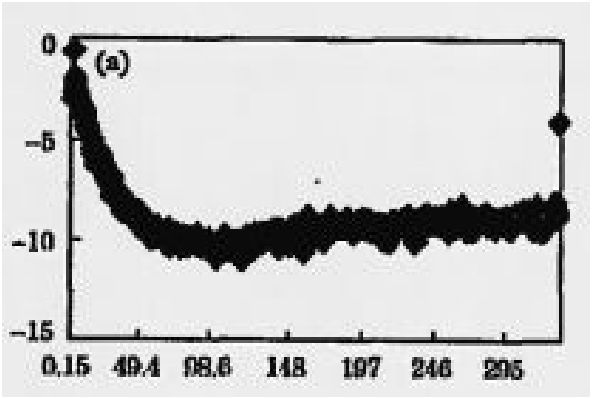

Fig. 2.17 Variation of diameter w.r.t. holding time [27].

Following this work, Basabe *et al*. in 2010 [28] carried out hot deformation torsion tests on a 0.036% Nb steel to investigate further the dynamic transformation of austenite into ferrite. They also discussed the industrial implications of dynamic transformation. They suggested that dynamically transformed ferrite was being formed in the finishing stages of hot rolling mills. This type of transformation appears to occur mainly in strip mills

because the interpass times are very short. By contrast in plate rolling and Steckel mill rolling, dynamic transformation plays a smaller role as the interpass times are longer. The addition of Nb to microalloyed steels decreases the level of reversion of the transformation, which may be useful in the rolling industry.

The 2012 research of Ghosh *et al*. [29] revealed that dynamic recrystallization and the dynamic transformation of austenite occurred simultaneously above the Ae_3 temperature. This was determined using the double differentiation method [30].

In this method [30], the 2% offset in the total strain, called the yield stress is first identified. This marks the initiation of work hardening and prior sections of the loading curve must be removed in order to study the onset of DRX and DT. This curve is then fitted using the MATLAB software, where the curve is smoothed to remove noise. This is carried out by fitting the curve with a high order polynomial equation. Next, the onset of DRX and DT are calculated by preparing θ (conventional strain hardening rate) versus σ (stress) curves. The critical condition is given by:

$$\frac{\delta}{\delta\sigma}\left(-\frac{\delta\theta}{\delta\sigma}\right) = 0 \qquad (1)$$

Now, the onset of DRX and the DT can be determined by plotting a $(-\partial\theta/\partial\sigma)$ vs σ curve and a θ vs σ curve. The latter corresponds to identifying the three inflection points in which the first and last points represent the onset of DT and DRX respectively. The second inflection point is the local maximum point, which represents a decrease in the rate of DT.

In **Ref. 29** discussed above, two minima were observed. The first and second minima, as already explained, refer to the initiation of dynamic transformation and dynamic

recrystallization. It was shown that larger strains are required for the ferrite to form at higher temperatures, where it is thermodynamically more unstable. On the other hand, the DRX mechanism displays the reverse tendency. The authors were able to account for DT ferrite formation at temperatures as high as 130 ºC.

2.4.1 Microstructural Analysis of Dynamically Transformed Ferrite

Under an optical microscope, when a typical low carbon steel (with a composition of 0.06%C, 0.30%Mn, 0.01%Si) is taken into its austenite region and deformed and quenched lath-like ferrite regions can be observed (**Fig. 2.18**). Note that in the micrographs, light regions are ferrite and darker regions martensite (prior austenite). It can be observed in the figure that the ferrite is nucleated within the austenite. This microstructure can be seen more clearly when the deformed samples are observed using the EBSD technique (**Fig. 2.19**). It is important to mention that the ferrite formed here is of the order of 200-300 nm wide so it cannot be detected using the conventional optical microscope.

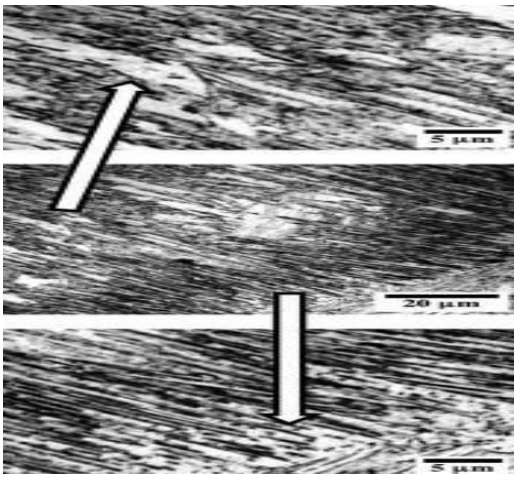

Fig. 2.18 Formation of martensite and DT ferrite as viewed under an optical microscope [31]. The darker regions represent martensite and the lighter ferrite.

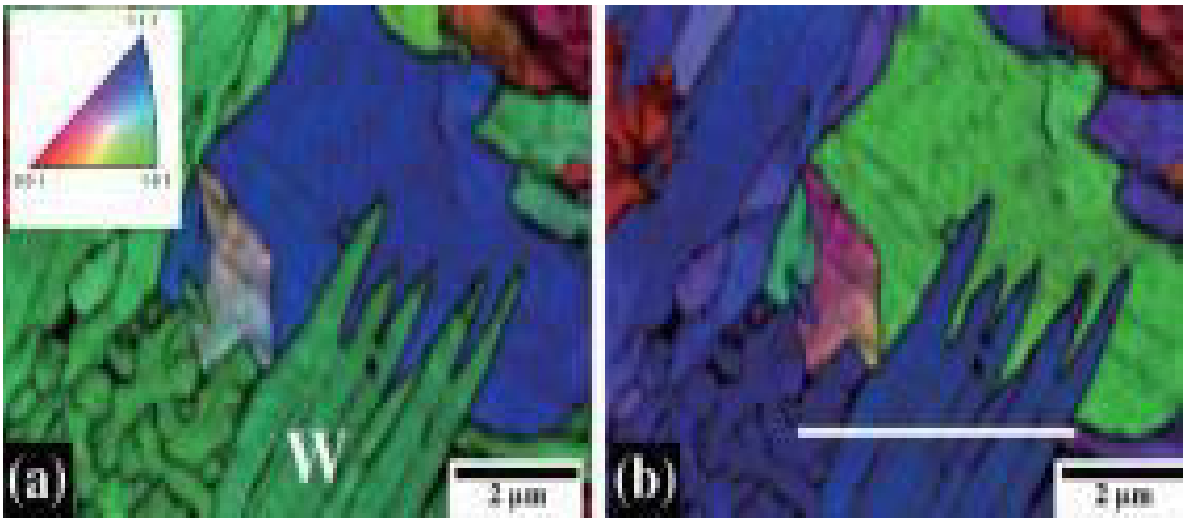

Fig. 2.19 Microstructure of Widmanstätten ferrite plates in a low carbon steel as viewed using EBSD techniques [31].

In another description of the effect of strain (0.4, 0.8, and 1.2) on the formation of DT ferrite, it was shown that the volume fraction of dynamically transformed ferrite increases with the strain. It was also reported that the plate volume fraction decreases with strain due to the coalescence of the plates into grains of polygonal ferrite. This process can be characterized as a recurring loop in which increasing the strain leads to the formation of DT ferrite plates, with the new plates coalescing into grains while the loop starts again [31]. This can be seen in the micrograph in **Fig. 2.20**.

2.4.2 Diffusion of Carbon During Dynamic Transformation

It is important to understand that carbon diffusion occurs during dynamic transformation. The diffusion of carbon occurs during or after dynamic transformation. Carbon diffusion can be studied by calculating the diffusion distances in austenite and ferrite. This can be expressed as:

$$\bar{X} = \sqrt{(D \times t)} \qquad (2)$$

Here, $\bar{X}$ is the mean distance of diffusion, D is the diffusivity of carbon, t is the time. Diffusivity is expressed as:

$$D = D_0 \exp(-Q/RT) \quad (3)$$

Here D_0, Q and T are the pre-exponential term, energy of activation, and temperature (in Kelvins), respectively, while R is the universal gas constant.

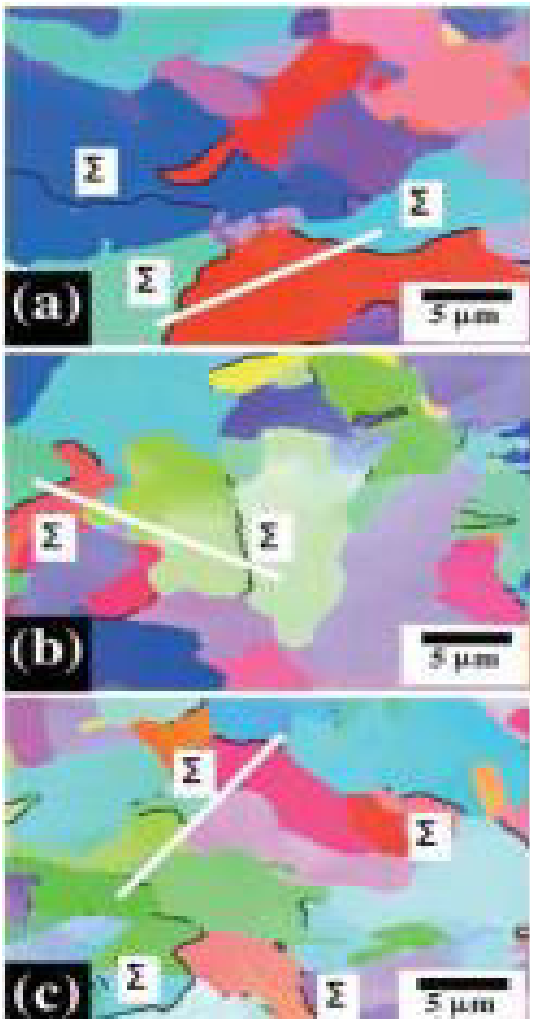

Fig. 2.20 IPF maps showing the effect of strain on the formation of DT ferrite a) ε = 0.4, b) ε = 0.8, c) ε = 1.2 [31].

Ghosh et al. [31] also calculated the carbon diffusion distance at 743-823 ºC. Their observations revealed that carbon took about 100 μs to diffuse a distance of 100 nm in ferrite. This was also the same time required for carbon to diffuse out of the Widmanstätten ferrite plates during DT. They also showed that substitutional elements, such as Mn, Si, could only diffuse a few nanometers during the same time period. This also proved that the forward transformation is displacive in nature and takes place under paraequilibrium conditions.

2.4.3 Effect of Gibbs Energy on the Phase Diagram

Ghosh *et al*. [31] showed that the extent of carbon diffusion in a particular steel depends on the amount of carbon present. If the steel has a carbon concentration below 0.15%, then there is no need for C diffusion and the Gibbs energy of the system undergoes an instant decrease. When the carbon levels are raised to 0.15% and 0.40%, carbon diffusion is almost instant (it takes of the order of 100 μs) but the reversion back into austenite takes a long time. On the other hand, when the carbon levels are above 0.40%, growth of the Widmanstätten ferrite plates is accompanied by parallel carbon diffusion and cementite precipitation. The conditions discussed above led to modifications in the conventional Fe-C phase diagram.

2.4.4 Dynamic Transformation Models

2.4.4.1 Stored Energy Transformation Model

In order to explain the rise in the Ae_3 line due to dynamic transformation, Ghosh et al. [31] introduced a model known as the stored energy transformation model (**Fig. 2.21**). According to this model, the stored energies of the dislocations lead to an increase in the Gibbs energy of the system, which in turn leads to the forward transformation of

austenite to ferrite. Upon further holding, the ferrite retransforms to austenite. However, this model could not explain why the forward transformation was faster than the reverse; and how low internal strains of only 10% can overcome the chemical free energy barrier.

2.4.4.2 Mechanical Activation Model

In order to overcome the discrepancies of the stored energy model, Jonas *et al*. (2013) [32] introduced three new concepts: i) the work of dilatation, ii) the work of shear accommodation, and iii) a driving force associated with the softening that accompanies the transformation. This modified model is shown in **Fig. 2.22**. In this model, above the Ae_3 temperature, the forward transformation is produced by mechanical activation and the stored energy. The magnitude of the latter energy is so small that it cannot overcome the free energy barrier opposing transformation as well as the dilatation work and the work of shear accommodation.

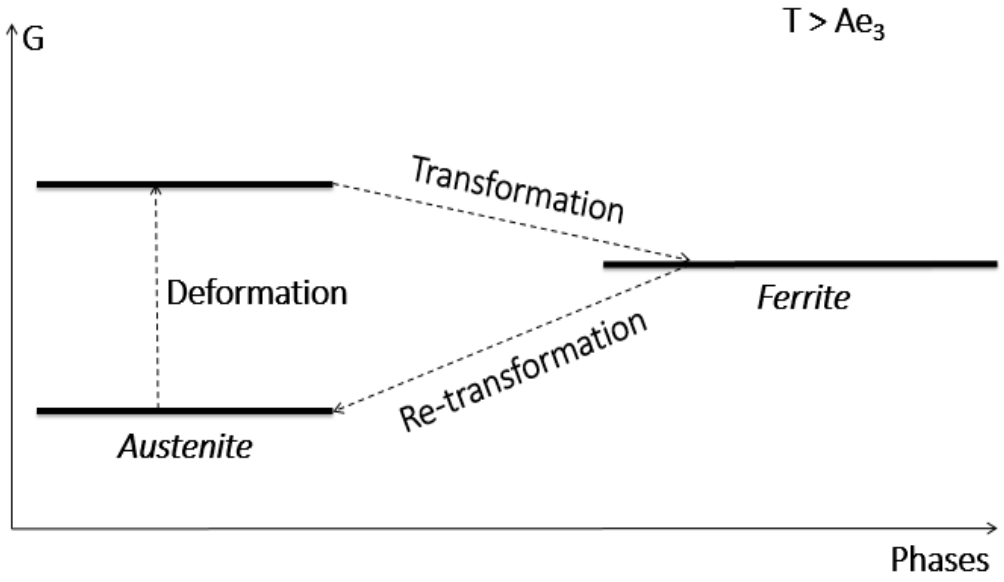

Fig. 2.21 Stored energy transformation model [32].

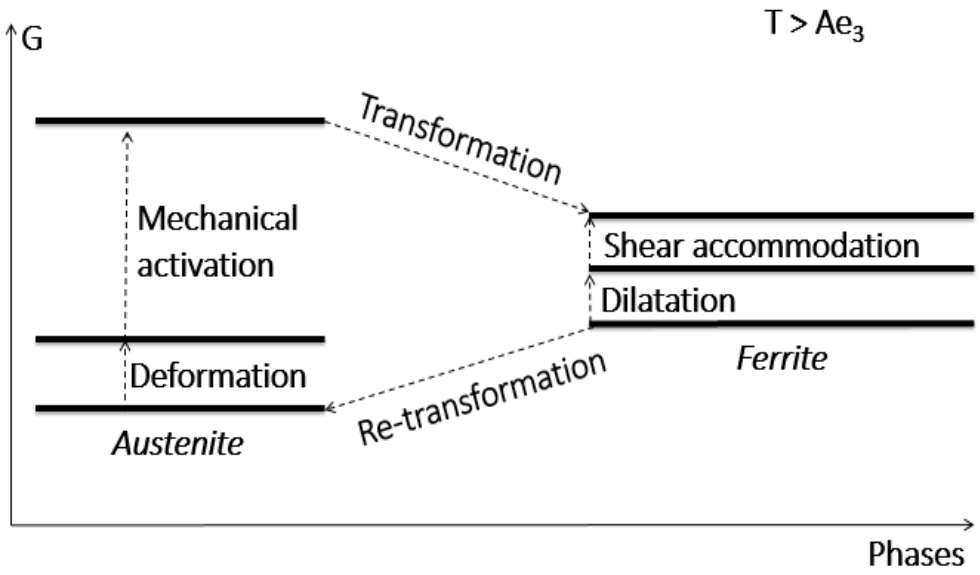

Fig. 2.22 Mechanical activation model [32].

The model also considered that the forward transformation is an athermal displacive process and occurs very rapidly, whereas the reverse transformation is thermally activated because it involves conventional iron atom diffusion. That is why the reverse transformation is much slower (many magnitudes slower) than the forward transformation [32].

2.4.4.2.1 Work of Dilatation

During dynamic transformation, dilatation occurs perpendicular to the habit plane. The austenite grains adjacent to the upper side of the expanding ferrite plates are forced to deform to make room for the plates. An illustration of this process is provided in **Fig. 2.23**. The work of dilatation per mol of austenite transformed can be calculated using the following equation:

$$W / V = \Lambda_1 * \sigma_{0.1} * \varepsilon \quad (4)$$

Here, $\sigma_{0.1}$ (at the point of nucleation) is the flow stress of the surrounding austenite and ε, the dilatation strain, is 0.03. The orientation factor, λ_1, in the most favorable case is cos 54.7 = 0.578. Therefore,

$$W/V = (0.578) * (\text{flow stress}) * 0.03 \text{ J/ mol} \quad (5)$$

2.4.4.2.2 Work of Shear Accommodation

The work of shear accommodation is best understood when pieces of self-accommodating plates are being formed, as illustrated in **Fig. 2.24**.

The austenite above and below the advancing plates remains unchanged but the austenite to the sides accommodates the shear. Thus, the work done per unit volume is:

$$W/V = \tau * \gamma = (m * \sigma_{0.1}) * 0.18 \quad (6)$$

where, m is the Schmid factor. The Schmid factor m for shear accommodation is cos λ_1 * cos λ_2; $\sigma_{0.1}$ is the flow stress at critical strain of 0.1; and γ is the average strain = 0.18 associated with the formation of Widmanstätten ferrite plates. Therefore,

$$W/V = (\cos \lambda_1 * \cos \lambda_2) * (\text{flow stress}) * 0.18 \text{ J/ mol} \quad (7)$$

2.4.4.3 Flow Softening Model for Dynamic Transformation

The mechanical activation model discussed in **Section 5.5.2** could only provide a qualitative explanation of the forward transformation. This resulted in the introduction of the flow softening model (**Fig. 2.25**). According to this model, the driving force for the transformation is provided by the softening that accompanies the transformation. This provides the energy required to overcome the barrier for transformation.

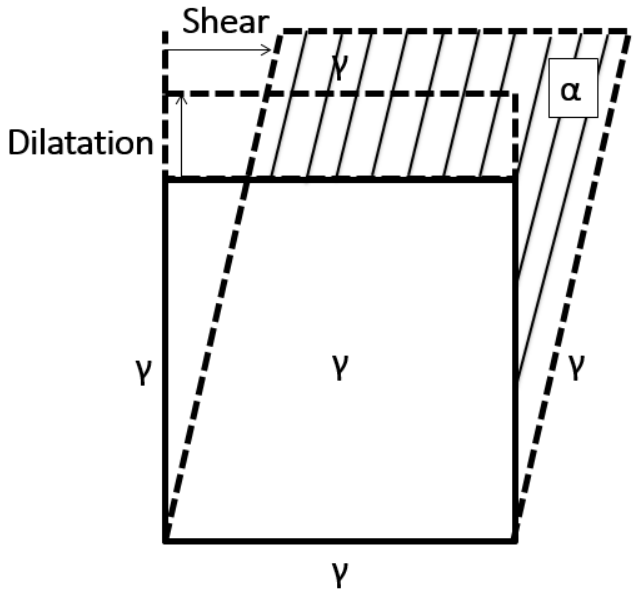

Fig. 2.23 Shape change involved in the transformation of austenite to ferrite via dilatation and shear [32].

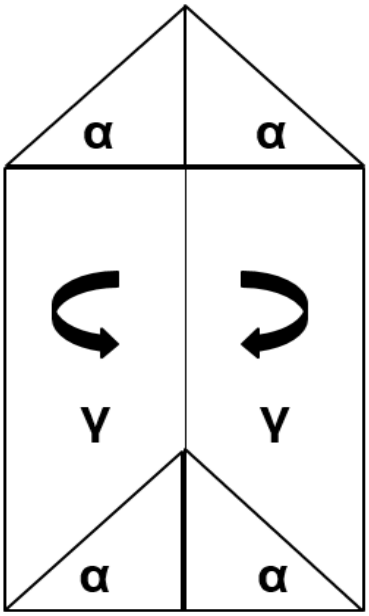

Fig. 2.24 The work of shear accommodation in the presence of self-accommodating plates [32].

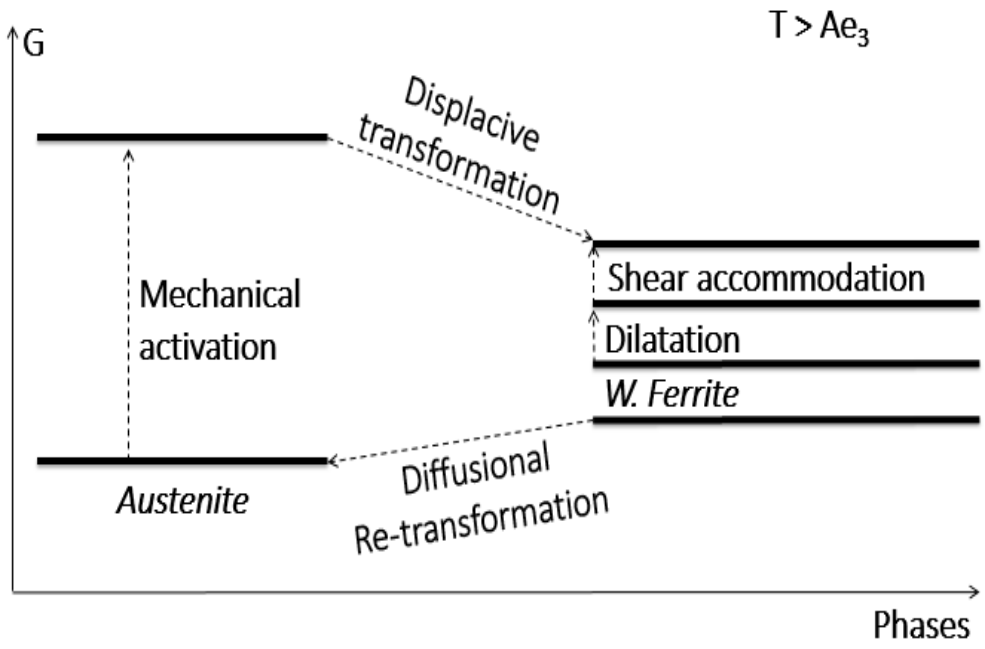

Fig. 2.25 Transformation softening model [33].

The amount of softening is deduced from the extrapolation of the flow stress of Widmanstätten ferrite along the inverse absolute temperature axis. The latter is calculated from the flow stress of Widmanstätten ferrite below the Ae_1. According to this model, a minimum critical strain must be attained so as to increase the driving force until it attains the value required to provoke the phase change [33, 34].

The main aim of the present investigation was to carry out compression tests on a 0.06wt%C-0.3wt%Mn-0.01wt%Si steel at temperatures high in the austenite phase field (up to 480 ºC above the $Ae_{3(p)}$ in the present case). Eight deformation temperatures were slected from 1000 to 1350 ºC (with intervals of 50º). The tests were carried out on a Gleeble 3800 thermodynamic simulator at École de Technologie Supérieure. Two different strains were employed, 0.3 and 0.65, while the strain rate was held constant at $1s^{-1}$. The water quenched samples were polished and etched before being studied

using optical microscopy and EBSD techniques. Double differentiation was also carried out to identify the critical strains for the initiation of dynamic transformation.

2.5 References

1. http://aarontan.org/MSE250/Images/Fig9_24.jpg
2. W.A. Soffa, D.E. Laughlin, “Chapter 8, Diffusional Phase Transformations in the Solid State, Physical Metallurgy,” (Fifth Edition) Vol. I (2014) 851.
3. http://cml.postech.ac.kr/2008/Steel_Microstructure/SM2.html
4. H.K.D.H. Bhadeshia, “Diffusional Formation of Ferrite in Iron and Its Alloys,” Progress in Materials Science, 29 (1985) 321-386.
5. H.K.D.H. Bhadeshia, “Chapter 21, Physical Metallurgy of Steels”, Physical Metallurgy (Fifth Edition) Vol. 3 (2014) 2157-2214.
6. R.F. Mehl, W.C. Hagel, “The Austenite: Pearlite Reaction,” Progress in Metal Physics, 6 (1956) 74-134.
7. http://lib.znate.ru/docs/index-107639.html
8. R.F. Mehl, “The Physics of Hardenability in Hardenability of alloy steels,” ASM, Cleaveland, Ohio (1939) 1-54.
9. R.F. Hehemann, “In Phase Transformations,” ASM, Metals Park, OH (1970) 397-432.
10. J. W. Christian, D.V. Edmonds,” Conf. on Phase Transformations in Ferrous Alloys,” ed. By A.R. Marder, J.I. Goldstein, TMS-AIME, Warrendale, PA (1984) 293-326.
11. M. Takahashi, H.K.D.H. Bhadeshia, “Model for Transition from Upper to lower Bainite,” Materials Science and Technology 6 (1990) 592-603.
12. H.K.D.H. Bhadeshia, “Bainite in Steels,” Institute of Materials, London (1992).

13. E.C. Bain, “Functions of the alloying elements in steel. American Society for Metals,” Metals Park, Ohio, USA (1939).
14. E.C. Bain, “The Nature of Martensite,” Trans. AIME 70 (1924) 25-46.
15. “Phase Transformations in Steels: Diffusionless Transformations High Strength Steels Modelling and Advanced Analytical Techniques, Diffusionless Transformations, High Strength Steels, Modelling and Advanced Analytical Techniques,” Woodhead Publishing Series in Metals and Surface Engineering, 2 (2012) 3.
16. http://www.msm.cam.ac.uk/phase-trans/2000/C9/lecture7.pdf
17. http://www.forgetechnology.com/db_files/56/14.jpg
18. R.D. Doherty, D.A. Hughes, F.J. Humphreys, J.J. Jonas, D.J. Jensen, M.E. Kassner, W.E. King, T.R. McNelley, H.J. McQueen, A.D. Rollett, “Current Issues in Recrystallization: a Review,” Materials Science and Engineering A, 238 (1997) 219-274.
19. Y.C. Lin, M.S. Chen, J. Zhong, “Study of Static Recrystallization Kinetics in a Low Alloy Steel,” Computational Materials Science, 44 (2008) 316-321.
20. F.H. Samuel, S. Yue, J.J. Jonas, K.R. Barnes, “Effect of Dynamic Recrystallization on Microstructural Evolution During Strip Rolling,” ISIJ International, 30 (1990) 216-225.
21. C. Ghosh, V.V.Basabe, J.J. Jonas, “Determination of the Critical Strains for the Initiation of Dynamic Transformation and Dynamic Recrystallization in Four Steels of Increasing Carbon Contents,” Steel Research Int, 84 (2013) 490-494.
22. W.B. Morrison, J. Iron and Steel Inst., 210 (1972) 618-623.

23. C. Roucoules, S. Yue, J.J. Jonas, “Effect of alloying elements on metadynamic recrystallization in HSLA steels”, Metall. Mater. Trans., A26 (1995) 181-192.
24. Y.C. Lin, M.S. Chen, J. Zhong,”Study of Metadynamic Recrystallization Behaviors in a Low Alloy Steel,” Journal of Materials Processing Technology, 209 (2009) 2477-2482.
25. Y. Matsumura, H. Yada, “Evolution Deformation of Ultrafine- Grained Ferrite in Hot Successive Deformation,” Transactions ISIJ, 27 (1987) 492-498.
26. H. Yada, C.M. Li, H. Yamagata, “Dynamic γ→α Transformation during Hot Deformation in Iron-Nickel-Carbon Alloys,” ISIJ international, 40 (2000) 200-206.
27. Y. Chen, Q. Chen, “Dilatometric Investigation on Isothermal Transformation after Hot Deformation,” J. Iron & Steel Res., Int., 10 (2003) 46-48.
28. V.V. Basabe, J.J. Jonas, “The Ferrite Transformation in Hot Deformed 0.036% Nb Austenite at Temperature Above the Ae_3,” ISIJ international, 50 (2010) 1185-1192.
29. C. Ghosh, V.V. Basabe, J.J. Jonas, “Determination of the Critical Strains for the Initiation of Dynamic Transformation and Dynamic Recrystallization in For Steels of Increasing Carbon Contents,” Steel Res. Int., 84 (2013) 490-494.
30. E. Poliak, J.J. Jonas, “A One-Parameter Approach to Determining the Critical Conditions for the Initiation of Dynamic Recrystallization,” Acta Materialia. 72 (2014) 13-21.
31. C. Ghosh, V.V. Basabe, J.J. Jonas, “Dynamic Transformation Behavior of Deformed High Carbon Steel at Temperatures Above the Ae_3,” ISIJ International. 53 (2013) 900-908.

32. J.J. Jonas, C. Ghosh, “Role of Mechanical Activation in the Dynamic Transformation of Austenite,” Acta Materialia, 61 (2013) 6125-6131.
33. C. Aranas Jr., J.J. Jonas, “Effect of Mn and Si on the dynamic transformation of austenite above the Ae_3 temperature,” Acta Materialia 82 (2015) 1-10.
34. C. Aranas, T. Nguyen-Minh, R. Grewal, J.J. Jonas, “Flow Softening-based Formation of Widmanstätten Ferrite in a 0.06%C Steel Deformed Above the Ae_3,” ISIJ International, 55 (2015) 300-307.

Chapter 3: Formation of Widmanstätten Ferrite Above 1000 ºC

Formation of Widmanstätten ferrite at very high temperatures in the austenite phase field

In this chapter, the formation of Widmanstätten ferrite is described at very high temperatures in the austenite phase field. For this purpose, experiments were carried out on a 0.06wt%C-0.3wt%Mn-0.01wt%Si steel over the temperature range from 1000 to 1350 ºC. The specimens were compressed on a Gleeble 3800 thermomechanical system to strains of 0.3 and 0.65 at the rate of 1 s^{-1}. Dynamic transformation was evident in all the tests and the volume fraction of ferrite first decreased until midway between the Ae_3 and the δ-ferrite phase field and then increased as the temperature approached the δ-ferrite phase field. Further, detailed microstructural examination by optical microscopy and EBSD techniques showed that Widmanstätten ferrite was present at all temperatures. As a result of the present observations, a modified Fe-C phase diagram is proposed for the case of dynamic loading. (See Appendix for corrected version.)

Formation of Widmanstätten ferrite at very high temperatures in the austenite phase field

Rupanjit Grewal[1], Clodualdo Aranas Jr.[1], Kanwal Chadha[2], Davood Shahriari[2], Mohammad Jahazi[2], John J. Jonas[1]

[1]Materials Engineering, McGill University

3610 University St., Montreal, Canada H3A 0C5

[2]Département de Génie Mécanique, École de Technologie Supérieure

1100 rue Notre-Dame Ouest, Montreal, Canada H3C 1K3

Abstract

Compression tests were carried out on a 0.06wt%C-0.3wt%Mn-0.01wt%Si steel at temperatures high in the austenite phase field. Eight deformation temperatures were selected in the range from 1000 to 1350 ºC at 50 ºC intervals. The quenched samples were examined using optical microscopy and EBSD techniques. It was observed that dynamic transformation took place and that the volume fraction of transformed ferrite first decreased with temperature (up to 1050 ºC) and then increased as the delta ferrite temperature domain was approached. The EBSD results revealed the presence of Widmanstätten ferrite plates under all testing conditions, right up to 1350 ºC. As a result of the present observations, a modified Fe-C phase diagram is proposed for the case of dynamic loading.

Keywords: thermomechanical processing, dynamic transformation, Widmanstätten ferrite

3.1 Introduction

The transformation of austenite to ferrite during deformation above the Ae_3 temperature was first studied by Yada and co-workers in the 1980's [1, 2]. In their pioneering work, Yada et al. showed that DT ferrite could be formed as high as 166 ºC above the Ae_3. They also demonstrated the occurrence of this unusual phenomenon in real time by performing in-situ X-ray examinations while simultaneously deforming by torsion testing [3]. Follow-up work by Chen and Chen in 2000 [4] showed that DT ferrite retransformed back into austenite on prolonged holding, 30 ºC above the Ae_3. More recently, researchers in various countries have reported on other aspects of the dynamic transformation of austenite [5-10].

The dislocation density introduced by working was initially taken to be the driving force for dynamic transformation. For example, Sun et al. [11] in 2008, calculated the Gibbs energy increase in the deformed system to be 22.3 $Jmol^{-1}$ and concluded that this was responsible for DT. Somewhat similar results were obtained by Hanlon et al. [12], who justified the presence of dynamically transformed ferrite in this way at temperatures up to 10 ºC above the Ae_3. Ghosh et al. [13] extended the temperature range proposed by Hanlon and co-workers [12] by allowing for the distribution of dislocations to be inhomogeneous in nature. By increasing the estimated local stored energy to 197 $Jmol^{-1}$, they were able to extend the predicted temperature range for the occurrence of this phenomenon up to 100 ºC above the Ae_3.

One limitation of the inhomogeneous distribution model is that it is unable to explain how strains as low as 10% can lead to the initiation of DT. This difficulty was resolved by

introducing the concept of mechanical activation by the applied stress, which can more readily account for the displacive nature of the forward transformation [14- 16]. In the most recent version of this approach, Aranas et al. [17- 19] proposed that the driving force for the transformation is the flow stress difference between the strain hardened austenite and the yield stress of the Widmanstätten ferrite that takes its place. As will be shown below, such softening can provoke dynamic transformation at temperatures right up to the upper limits of the austenite phase field.

The objective of the present investigation was, therefore, to determine the characteristics of dynamic transformation at temperatures very high in the austenite phase field (up to 480 ºC above the $Ae_{3\,(p)}$ in the present case). For this purpose, compression tests were performed on a 0.06wt%C-0.3wt%Mn-0.01wt%Si steel using a Gleeble 3800 thermomechanical system. The tests were conducted in the temperature range 1000 to 1350 ºC (with intervals of 50º). Strains of 0.3 and 0.65 were employed in the tests and the strain rate was held constant at $1s^{-1}$. After water quenching, the specimens were polished and etched for examination by means of optical and electron back scattered microscopy. Double differentiation was also employed to identify the critical strains necessary for the initiation of dynamic transformation. The present observations indicate that the Fe-C phase diagram must be modified so as to apply to the case of dynamic loading.

3.2 Experimental Procedure

3.2.1 Compression testing

The plain C-Mn steel was received in the form of hot rolled plates with thicknesses of 12.5 mm. Cylindrical compression samples with dimensions of 15 mm X 10 mm were machined from these plates with the cylinder axes parallel to the rolling direction. The composition of this alloy is shown in **Table 3.1** together with the respective paraequilibrium and orthoequilibrium Ae_3 temperatures [13]. These were calculated using the FSStel database of the FactSage [20] and were validated using the Thermo-Calc thermodynamic software [21].

C	Mn	Si	Orthoequilibrium Ae_3	Paraequilibrium Ae_3
0.06	0.30	0.01	877 ºC	870 ºC

Table 3.1 Chemical composition (weight %) and equilibrium transformation temperatures (ºC)

The compression tests were carried out in a vacuum and the Gleeble 3800 (Dynamic Systems Inc. USA) thermomechanical simulator was interfaced with QuikSim software that controlled the heating rate, cooling rate, quenching medium, strain, strain rate and temperature. The thermomechanical schedule employed is displayed in **Fig. 3.1**. Here the specimens were heated at the rate of 4.5 ºC s^{-1} to test temperatures in the range 1000 ºC to 1350 ºC and held for 3 minutes in order to fully austenize the microstructure before deformation. These were water quenched immediately after straining. Note that, a K-type thermocouple was used for the experiments carried out over the range 1000 ºC to 1250 ºC. For the compression tests above 1250 ºC, an R-type thermocouple was employed.

The data were later processed into stress vs strain curves directly by the above software. The first set of compression tests involved the imposition of a strain of 0.3 applied at the rate of 1 s^{-1} over the temperature range 1200 to 1350 ºC. In the second set, a higher strain of 0.65 was applied using the same parameters, but over the wider temperature range 1000 to 1350 ºC. Note that these temperatures are high in the austenite phase field and approach the delta ferrite formation temperature of approximately 1472 ºC.

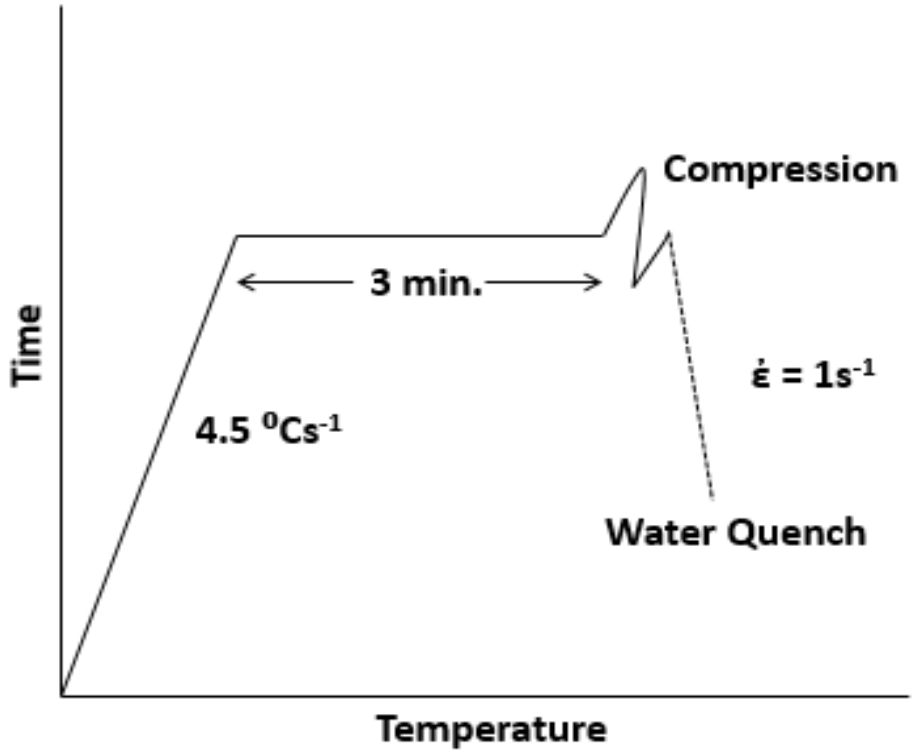

Fig. 3.1 Thermomechanical schedule of the compression tests carried out to strains of i) 0.3 at temperatures in the range from 1200 – 1350 ºC and ii) 0.65 in the range 1000 – 1350 ºC. The strain rate was 1s^{-1} in both series of tests.

3.2.2 Metallography

For microstructural examination, central cross-sections perpendicular to the longitudinal axis were cut from the compressed specimens. The latter were then mounted in a phenolic hot mounting resin. The mounted specimens were polished using SiC papers from 400 to 1200 grit. Finally, these were subjected to 3 and 1 μm diamond polishing. Thereafter, the specimens were etched with 2% nital for optical microscopy. For determination of the volume fraction of DT ferrite in the austenite, etching was also carried out using a 10% sodium metabisulfite ($Na_2S_2O_5$) solution. MIP microstructure analysis software was then used to calculate the volume fractions.

For the EBSD analysis, the specimens from each temperature were polished in the same manner as was employed for optical microscopy. Later, the specimens were subjected to final polishing using 0.05 μm silica in a vibromet for 6 to 8 hours.

3.3 Results

The stress-strain curves associated with deformation over the temperature range 1000 to 1350 ºC are displayed in **Fig. 3.2**. Here the samples were strained to 0.65 at the rate of 1 s^{-1}. All the curves display softening after the peak stress is attained. As shown by earlier workers [6, 14] this is due to the concurrent operation of dynamic transformation and dynamic recrystallization. Steady state flow was attained at a strain of about 0.4. An interesting feature of these curves is their somewhat “flattened” shape prior to the peak. This is an indication of the initiation of dynamic transformation, which reduces the net rate of strain hardening once it is underway.

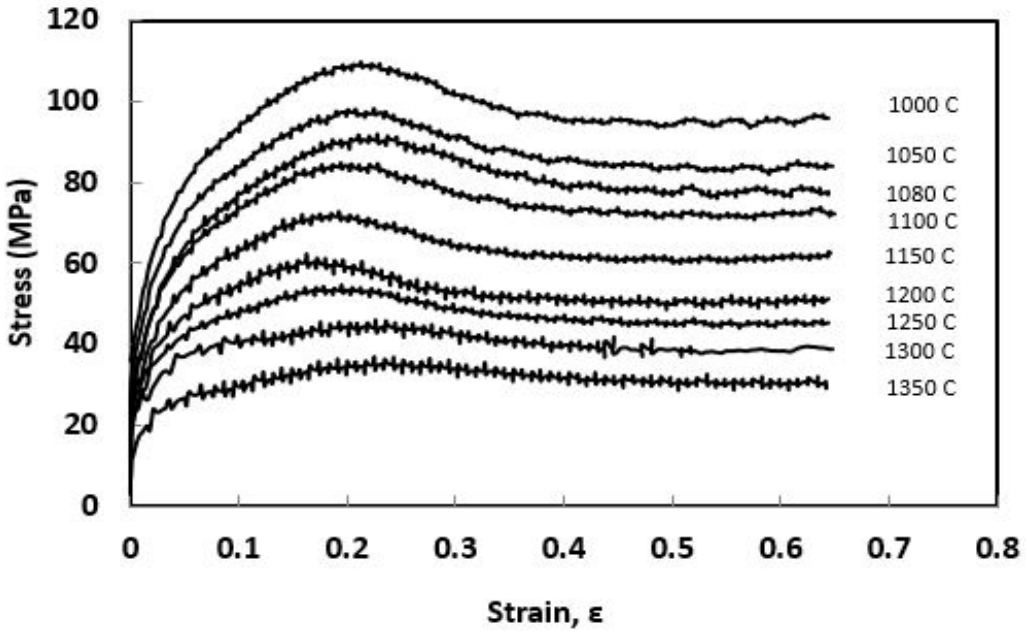

Fig. 3.2 Stress vs strain curves of the 0.06wt% C- 0.3wt% Mn- 0.01wt% Si steel compressed to a strain of 0.65 at $1s^{-1}$ over the temperature range 1000 to 1350 ºC. Flow softening of about 10% is generally observed after the peak stress is attained.

The transformation softening process makes it possible to detect its initiation by means of the double differentiation technique, as will be shown in more detail below.

3.3.1 Mean Flow Stress

The areas under the flow curves of **Fig. 3.2** were determined by integrating up to a strain of 0.65. The mean flow stresses derived from these areas are illustrated in **Fig. 3.3**, where they are plotted against inverse absolute temperature. Here, it can be seen that they extrapolate to a value of 4-5 MPa at the melting temperature. Thus the present high temperature measurements validate the frequent assumptions of earlier workers [18, 19] that lower temperature measurements can be extrapolated in a linear manner (against 1/T) right up to the melting point.

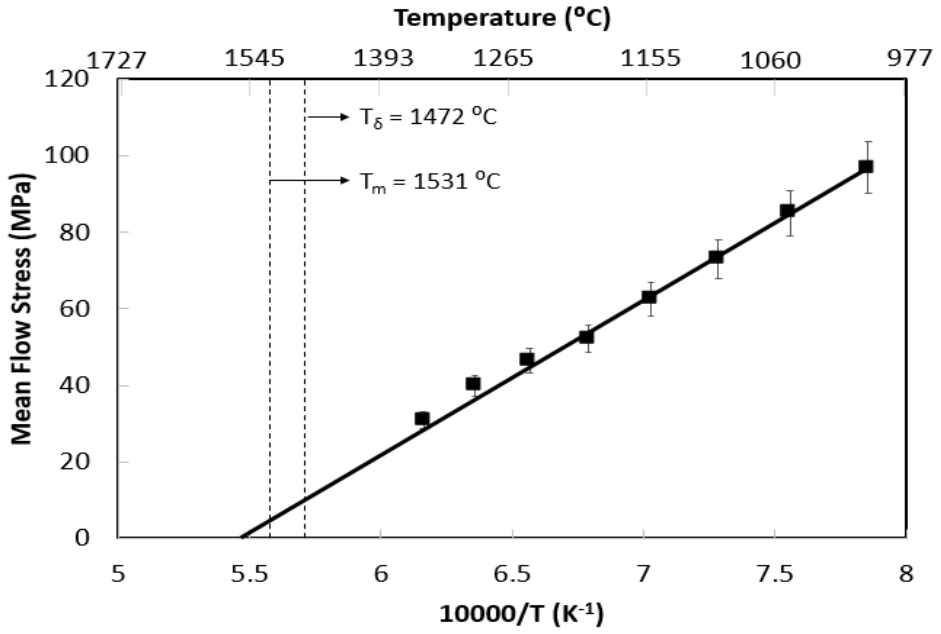

Fig. 3.3 Mean flow stresses calculated from the stress-strain curves of **Fig. 3.2** for the 0.06wt%C-0.3wt%Mn-0.01wt%Si steel.

3.3.2 Critical strains for the initiation of dynamic transformation

Double differentiation was applied to the flow curves of **Fig. 3.2** using the MATLAB software [22]. Most of the curves were fitted using a 9th order polynomial, although in the higher temperature cases, a higher-order polynomial was used. This method is illustrated in **Fig. 3.4**, where the strain hardening rate (Θ) is first defined, **Fig. 3.4a**. The dependence of Θ on σ is plotted in **Fig. 3.4b**, which shows the two inflection points that correspond to the moments of initiation of dynamic transformation and dynamic recrystallization. The locations of these points were then determined more precisely by noting that they correspond to the following condition:

$$\frac{\delta}{\delta\sigma}\left(\frac{\delta\theta}{\delta\sigma}\right) = 0 \qquad (1)$$

The two minima seen in the plot of (-∂Θ/ ∂σ) against stress displayed in **Fig. 3.4c** obey this condition. These minima represent the critical stresses at which dynamic transformation and dynamic recrystallization are initiated during deformation. The critical strains that correspond to these stresses were then evaluated by referring back to the initial flow curves, **Fig. 3.2** [23].

The critical stresses determined in this way over the temperature range 1000 ºC to 1350 ºC are shown in **Fig. 3.5a**. Both of these decrease with temperature [19]. The critical strains that correspond to these stresses are illustrated in **Fig. 3.5b**. Here the critical strains for DRX decrease with increasing temperatures in the normal way [19]. By contrast, the DT critical strains first increase with temperature to a maximum and then decrease as the delta ferrite phase field is approached. The average values for the DT and DRX critical strains are about 0.08 and 0.15, respectively.

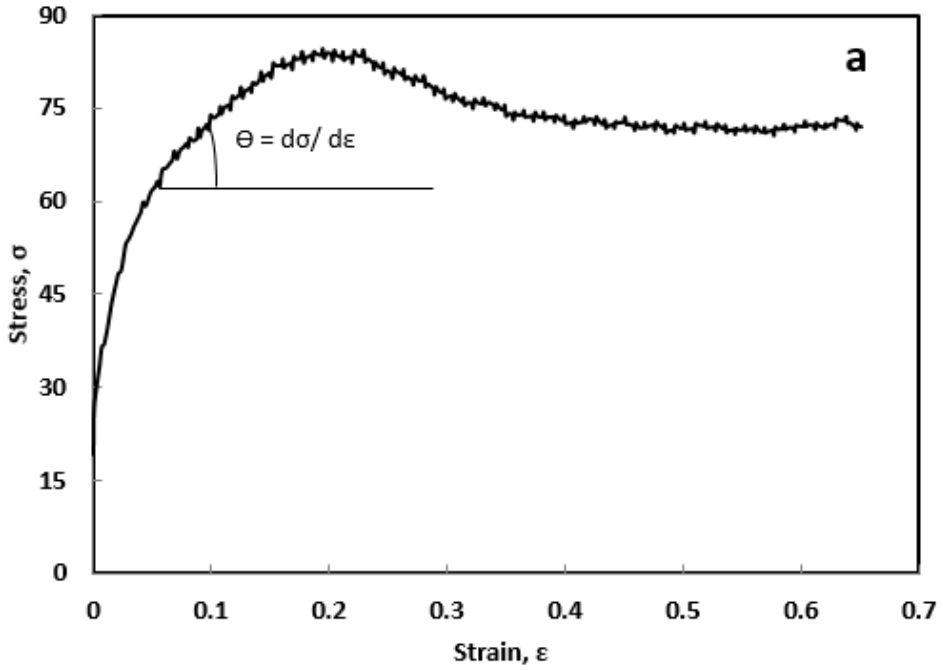

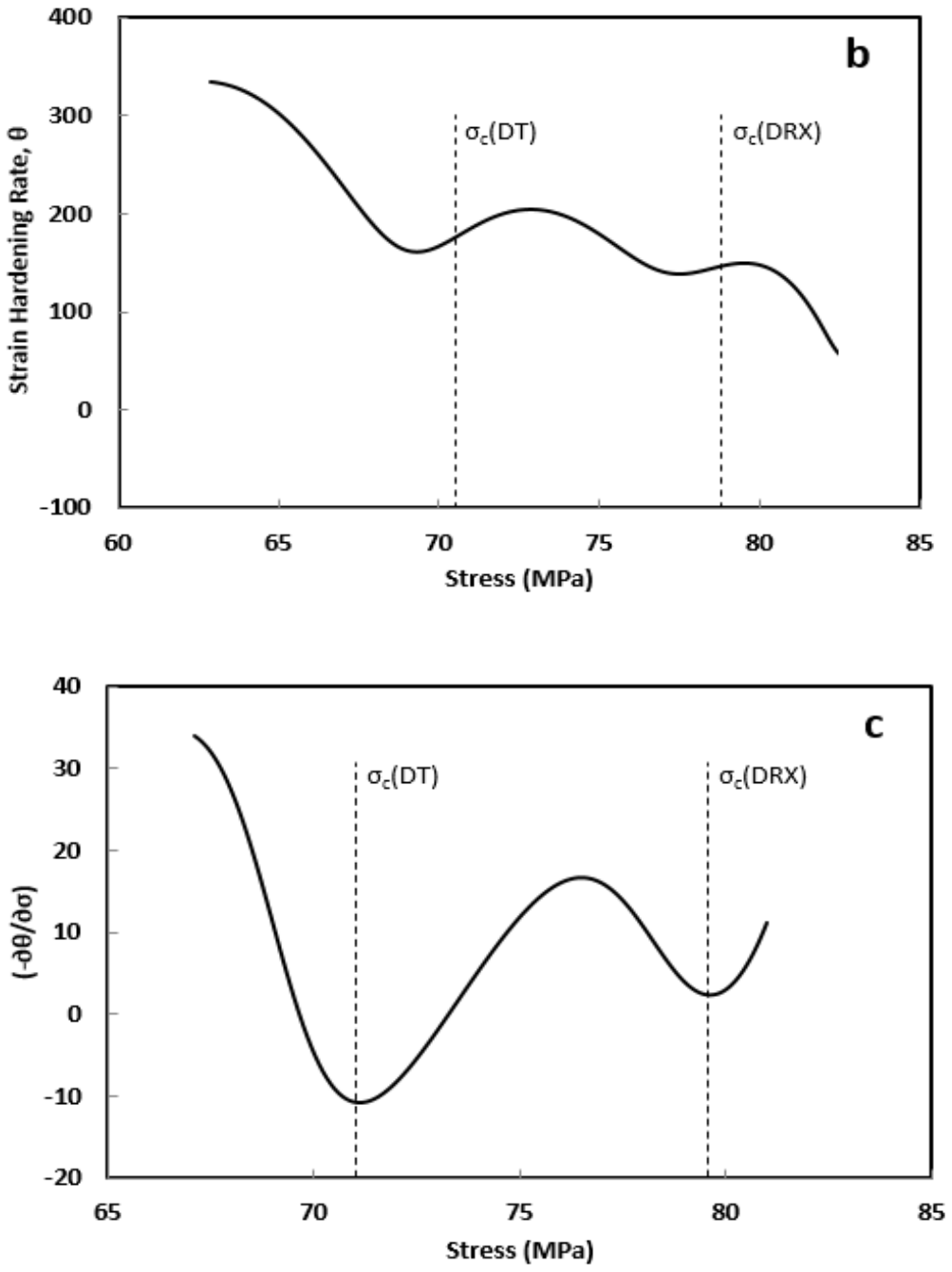

Fig. 3.4 The double differentiation method employed in determination of the critical stresses and strains: a) definition of the strain hardening rate; b) plot of Θ vs stress illustrating the presence of two (of the three) inflection points; and c) examples of the dependence of (-∂Θ/∂σ) on stress. This experiment was carried out at 1100 ºC.

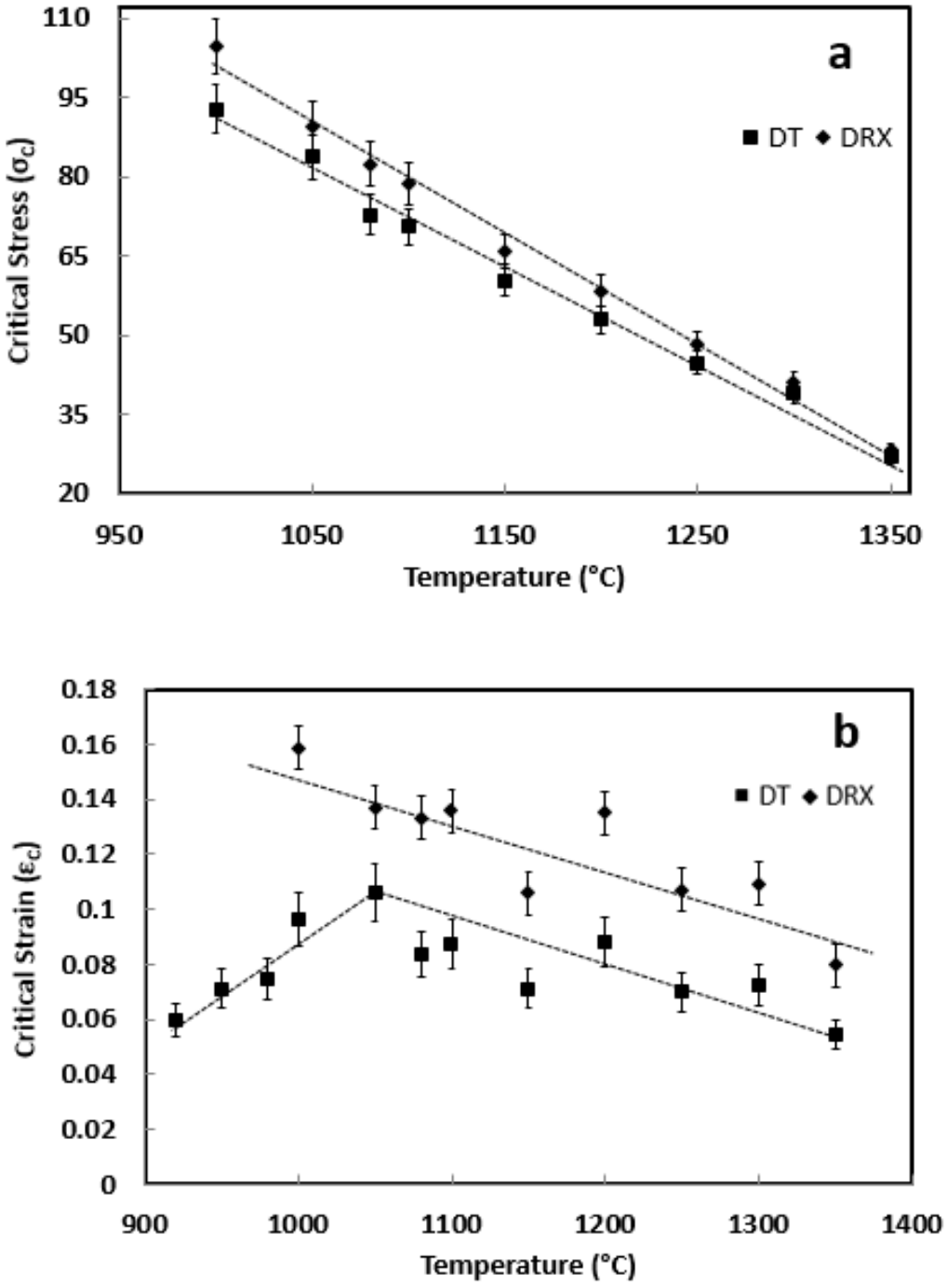

Fig. 3.5 a) Critical stresses for dynamic transformation (DT) and dynamic recrystallization (DRX) determined over the temperature range 1000 to 1350 ºC; b) critical strains over the same temperature range.

3.3.3 Dynamic transformation microstructures

As demonstrated in more detail elsewhere [16, 19], dynamic transformation involves the initial formation of near-identically oriented Widmanstätten ferrite plates followed by their coalescence into polygonal grains. In order to check if this sequence of events was followed at the much higher temperatures employed here, optical microscopy was performed on the samples deformed to the lower strain of 0.3. Examples of the colonies of ferrite plates formed under the present conditions are shown in **Fig. 3.6**. Here, the darker regions correspond to martensite (prior austenite) and the lighter regions to ferrite. It can be seen that the volume fraction of Widmanstätten ferrite increases with temperature, as will be demonstrated in more detail below. There is also a tendency for the plate width to increase with temperature. It should be noted that the ferrite plates formed are mostly along the grain boundaries of the prior austenite, although plates can also nucleate within the grains [13, 15].

In order to support the above interpretation of the microstructure, Vickers hardnesses were measured in selected regions in the samples strained to 0.3. Examples of the values obtained in the 1200 to 1350 ºC samples are presented in **Fig. 3.7**. These values are consistent with the results obtained in tests carried out below 1000 ºC [24]. Here, the average polygonal ferrite microhardness was about 170 HV and that of the martensite was 263 HV. The latter value is consistent with martensite hardness values in the range 200 – 300 HV expected in low C steels [25]. By contrast, the hardness of the Widmanstätten ferrite plates was somewhat higher than for polygonal ferrite at 203 HV vs. 174 HV, as seen in the sample deformed at 1300 ºC (**Fig. 3.7c**).

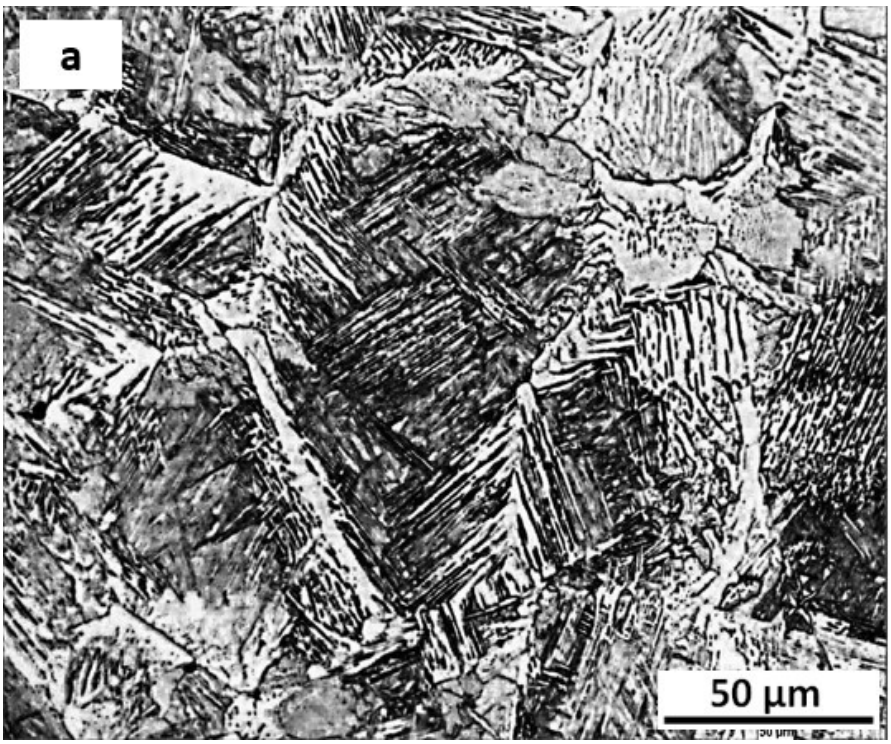
a
50 µm

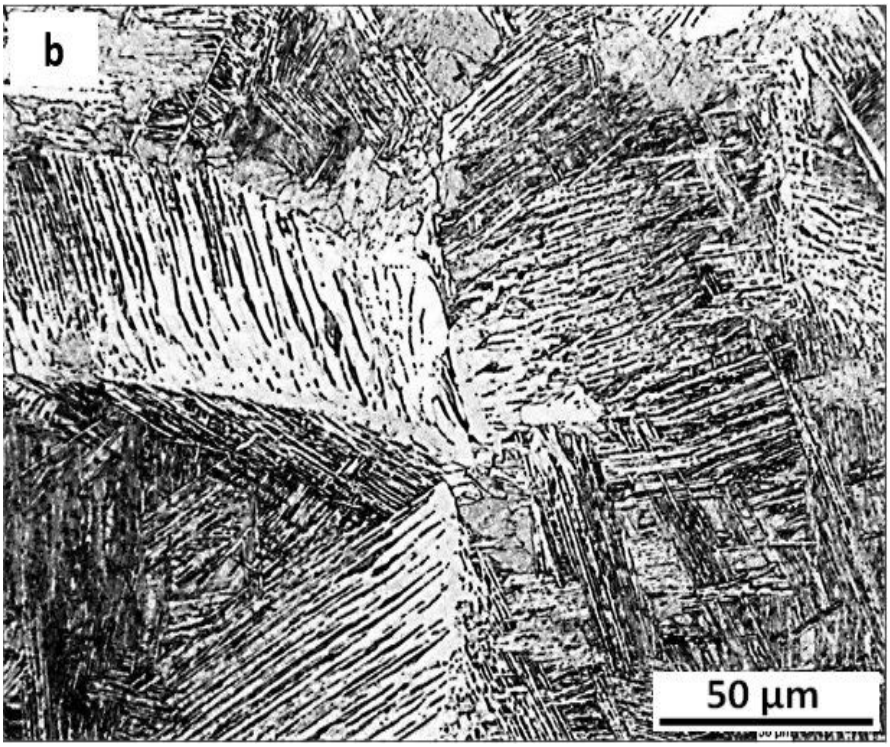
b
50 µm

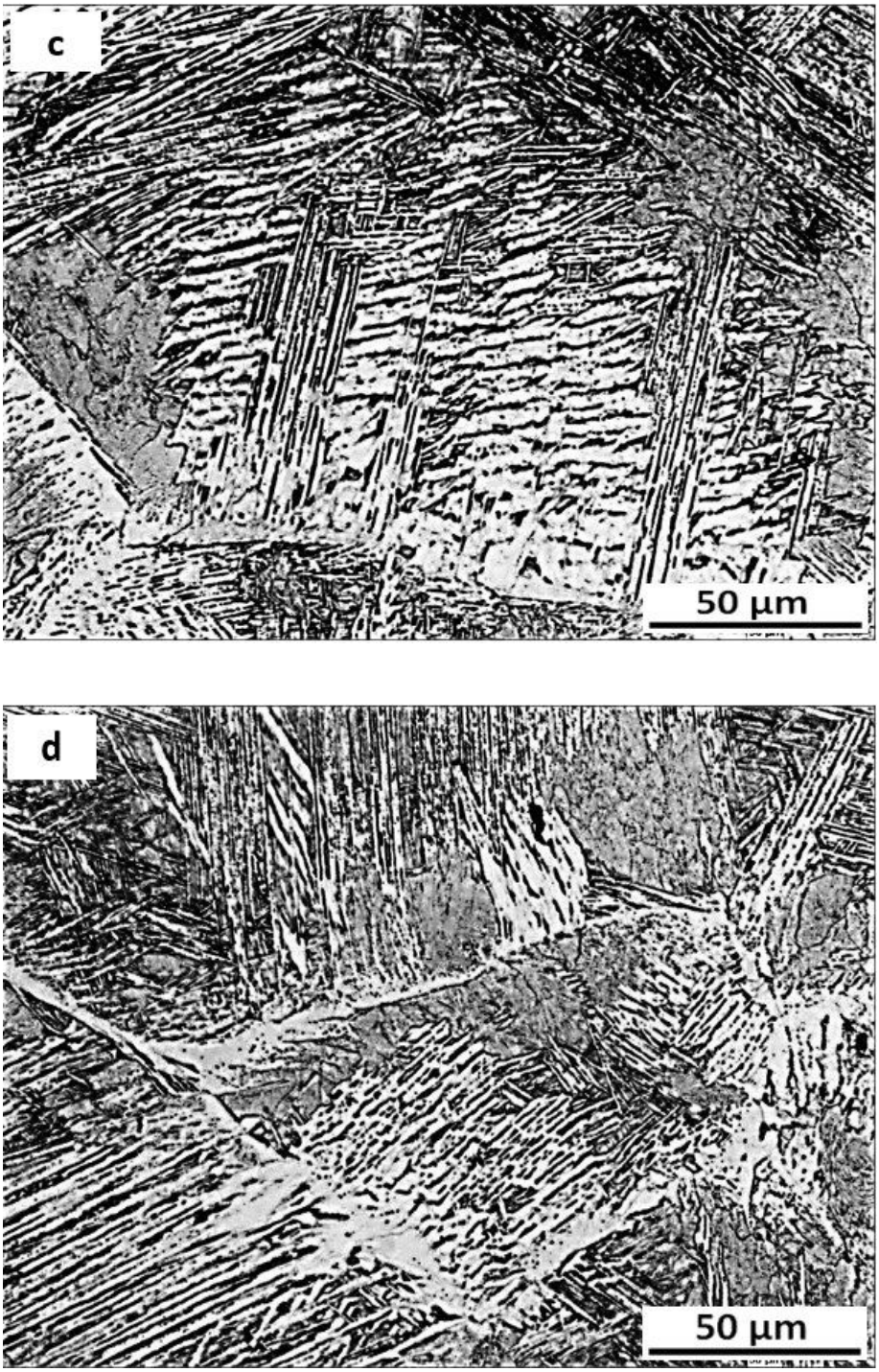

Fig. 3.6 Optical micrographs at 500X of the present steel compressed to a strain of 0.3 at 1s^{-1}: a) 1200 ºC b) 1250 ºC c) 1300 ºC d) 1350 ºC. The dark regions are martensite

(prior-austenite) and the lighter ones are ferrite. The formation of plate-like Widmanstätten ferrite is evident even at 1350 ºC.

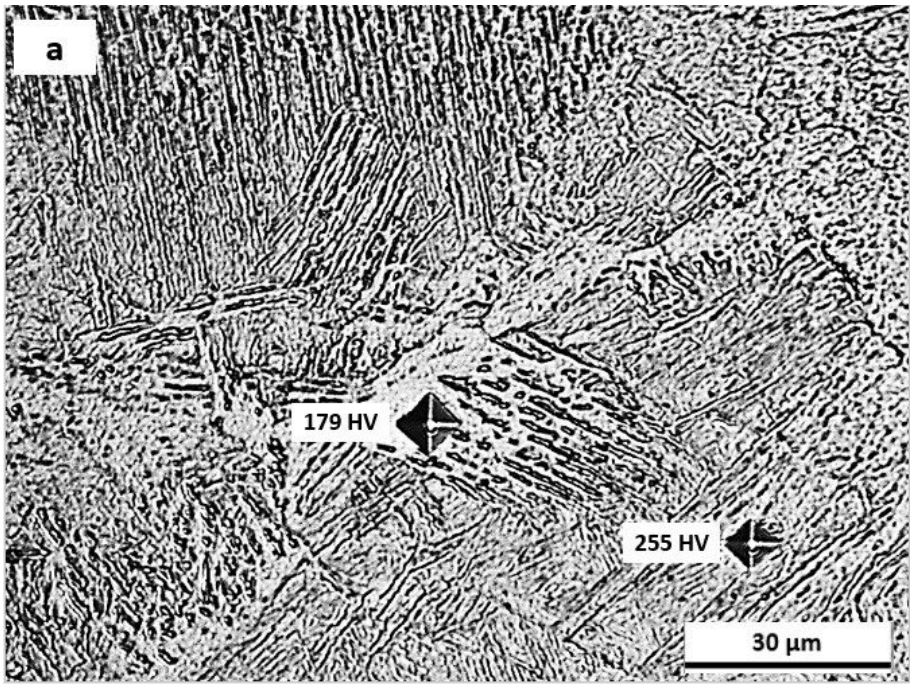

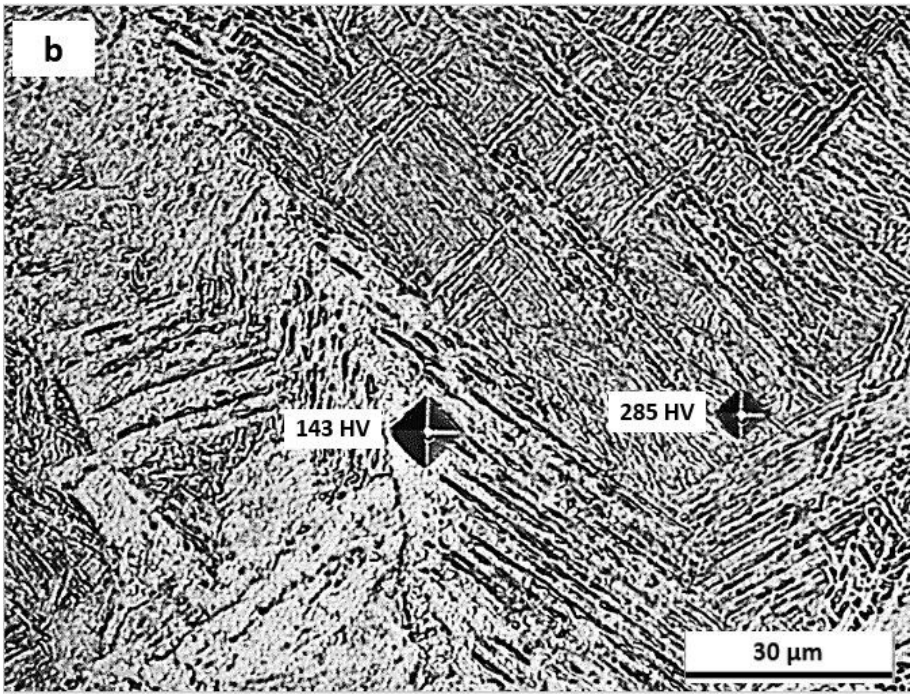

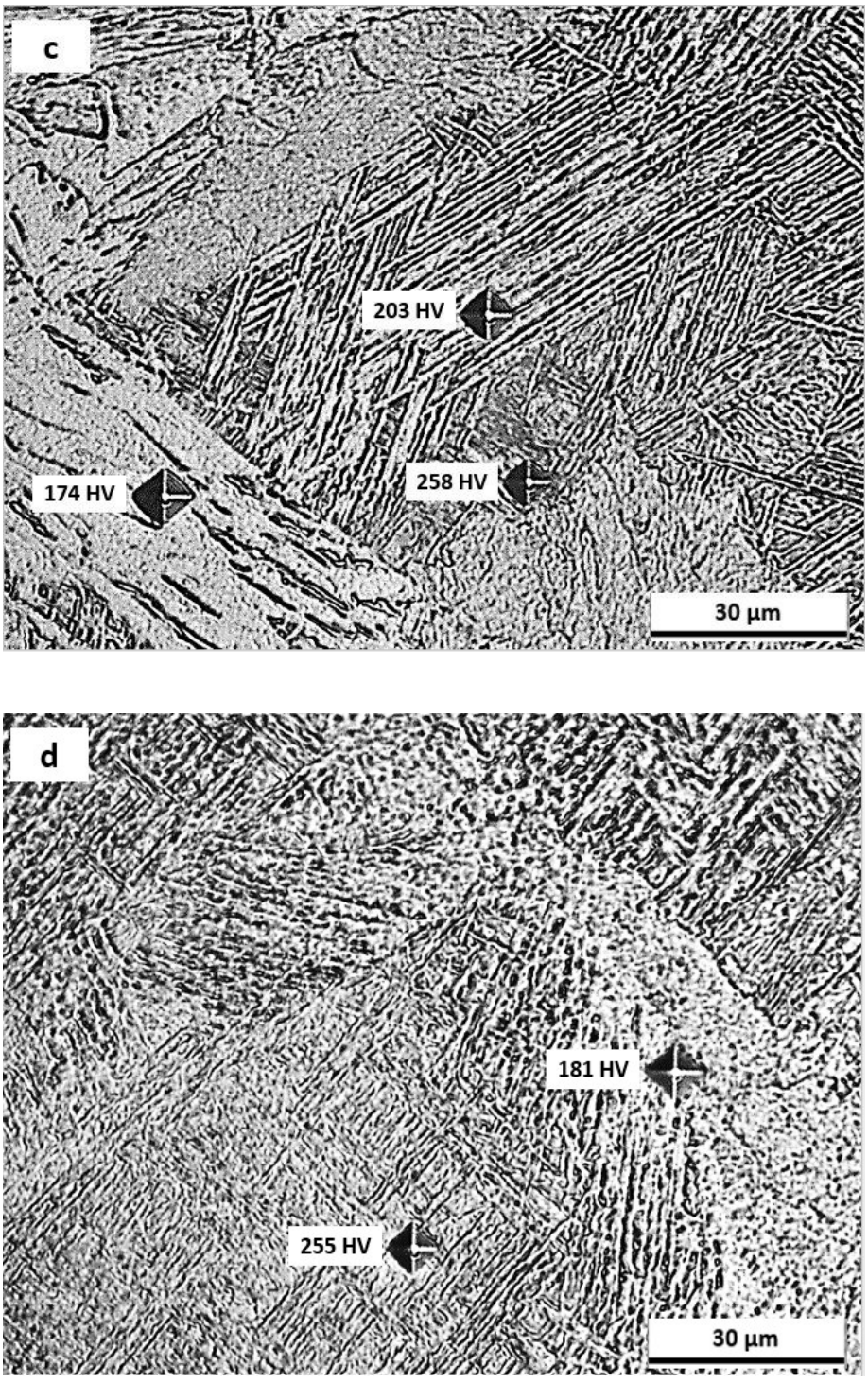

Fig. 3.7 Vickers microhardnesses of the polygonal ferrite, Widmanstätten ferrite and martensite (prior-austenite) in samples strained to 0.3 at a) 1200 ºC b) 1250 ºC c) 1300 ºC d) 1350 ºC.

The microstructures associated with the samples deformed to a strain of 0.65 are illustrated in **Fig. 3.8**. Here appreciable amounts of ferrite are present, which are homogeneously distributed throughout each specimen. The volume fraction of DT ferrite was calculated using the MIP software and at least 15 micrographs were scanned for each condition for this purpose. As mentioned earlier, the darker and lighter regions correspond to martensite (prior austenite) and ferrite, respectively.

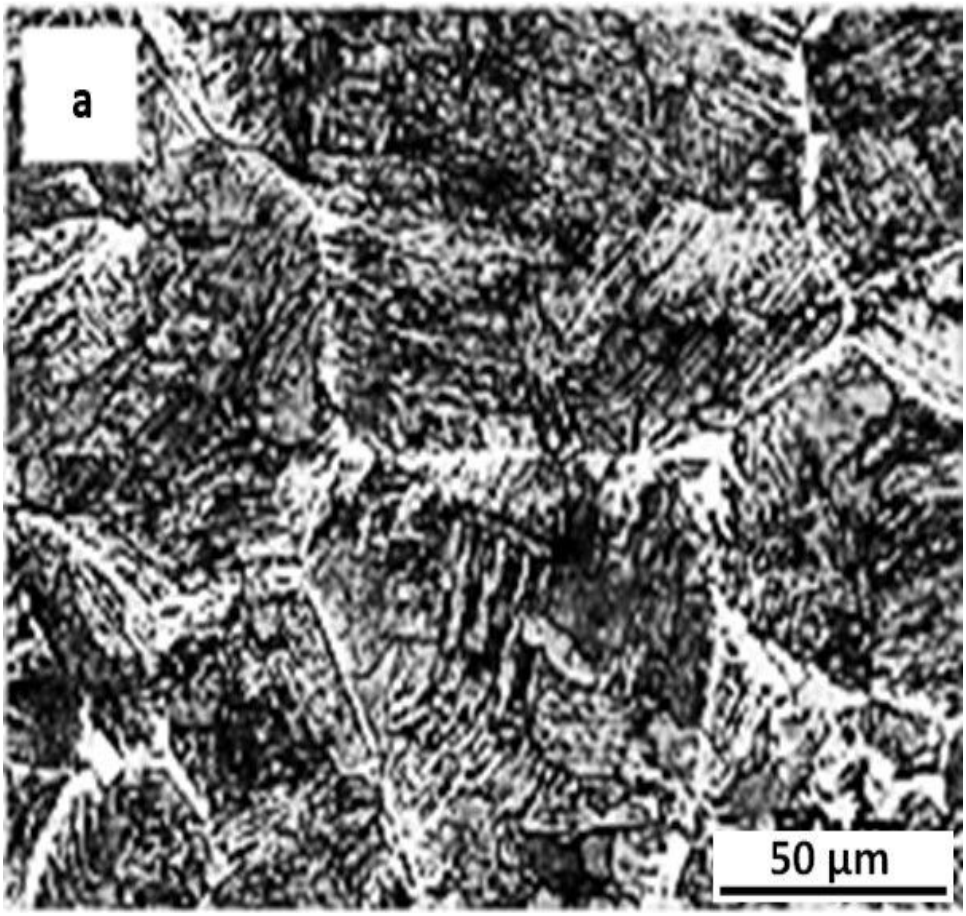

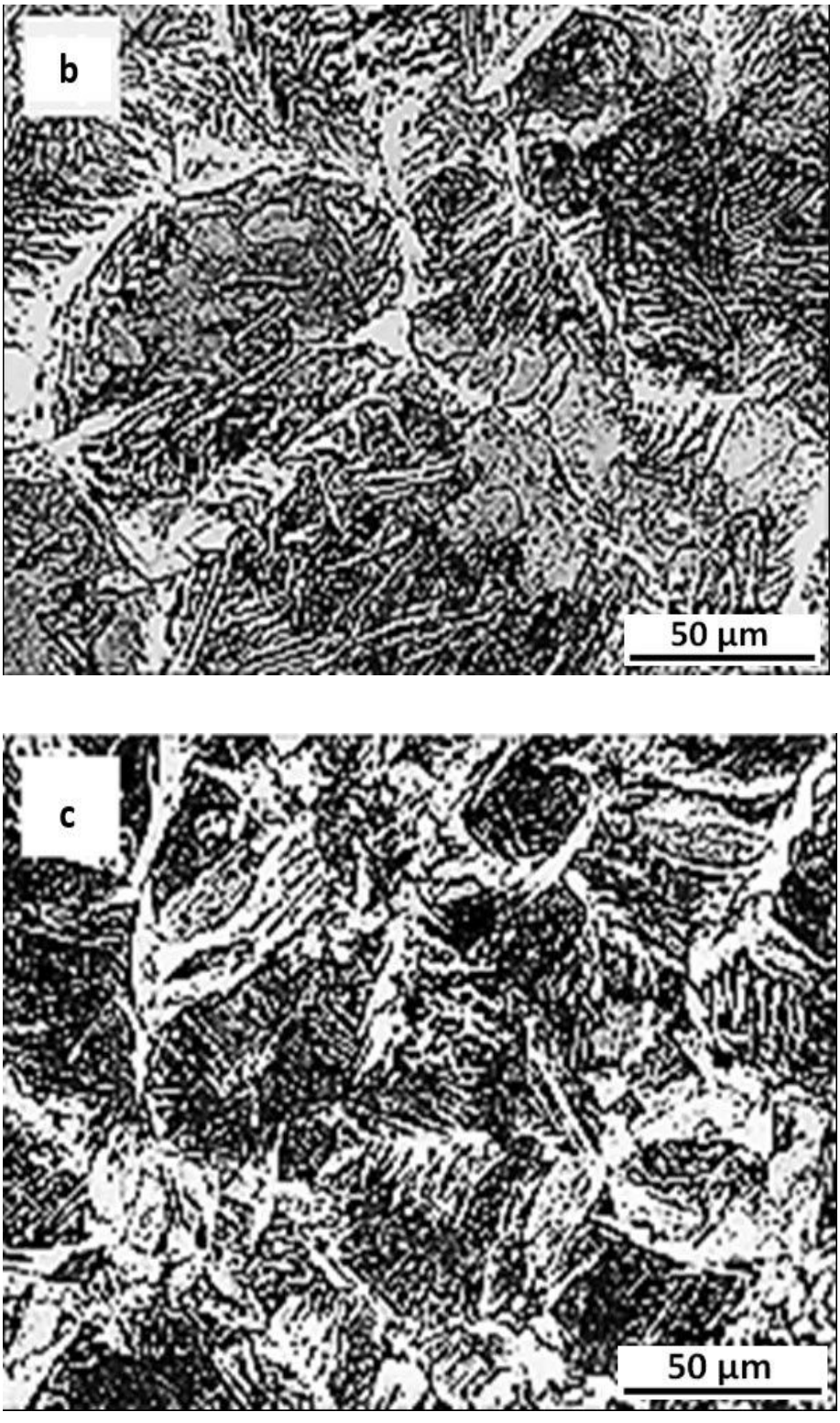

Fig. 3.8 Optical micrographs of the present steel compressed to a strain of 0.65 at 1s^{-1} at: a) 1050 ºC b) 1150 ºC c) 1200 ºC. The volume fraction of ferrite increases with

temperature. The darker and lighter regions correspond to martensite (prior austenite) and ferrite, respectively.

The result of these measurements are displayed in **Fig. 3.9**. Here, it can be seen that the volume fraction of ferrite first decreases to a minimum of about 10% at 1050 ºC. It then increases with temperature to about 25% at 1200 ºC.

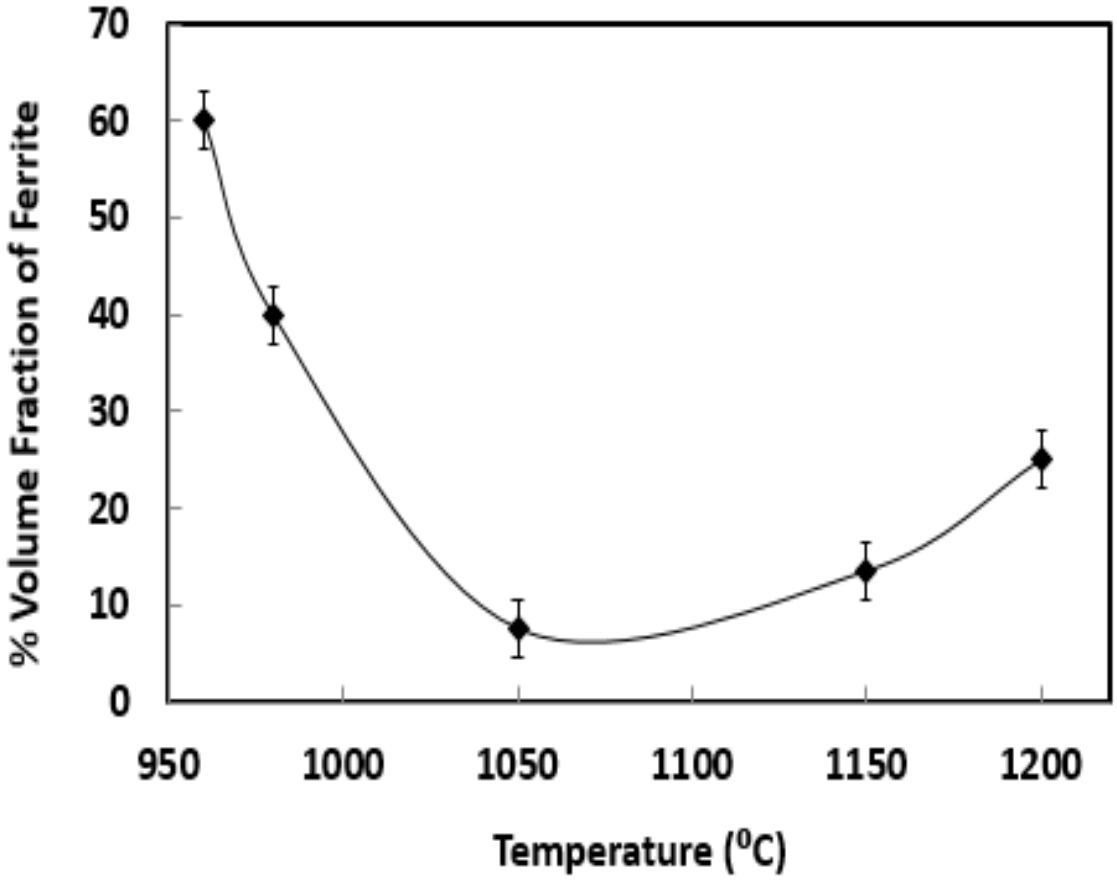

Fig. 3.9 Volume fraction of ferrite vs temperature at a strain of 0.65. The volume fraction is lowest (about 7.5 %) midway between the Ae_3 and the δ-ferrite phase field.

3.3.4 High magnification (EBSD) microstructures

The optical micrographs in the previous section indicated that Widmanstätten ferrite plates continued to be formed in the samples deformed at the highest temperatures in the austenite phase field. The orientations of these plates were characterized by means of the electron backscattered diffraction (EBSD) technique. An inverse pole figure map of some of the plates formed at 1200 ºC ($Ae_{3\,(p)}$ + 330 ºC) is illustrated in **Fig. 3.10a**. This sample was strained to ε = 0.3 at 1 s^{-1}. Here, the black regions are martensite (prior austenite) and the plates can be seen to be present in colonies of similar orientation [26].

On increasing the magnification to 7500X **(Fig. 3.10b)**, the plates can be seen more clearly. Their widths fall in the range 1 – 2 μm; these are nearly an order of magnitude thicker than the 200 nm plates formed at 900 – 1000 ºC [26, 27]. The coalescence of the plates into polygonal ferrite is illustrated in **Fig. 3.10c** for ε = 0.65 at 1 s^{-1}. It is likely that the coalesced plates of **Fig. 3.10c** were formed early in this experiment, for instance at a strain of 0.10 to 0.15, while the 'fresh' plates of **Fig. 3.10b** were formed closer to the final experimental strain of 0.3, e.g. at ε = 0.25 to 0.30.

The widening of the plates is probably associated with the increased diffusivity of C in ferrite over this temperature range. This hypothesis can be evaluated by calculating the carbon diffusion distance under the present conditions. This is specified by the following relationship:

$$\bar{X} = \sqrt{(Dt)} \qquad (2)$$

where $\overline{X}$ is the mean diffusion distance, D the carbon diffusion coefficient in ferrite and *t* the time. The diffusion coefficient is in turn given by:

$$D = D_0 \exp(-Q/RT) \qquad (3)$$

where $D_0 = 7.9 \times 10^{-3}$ cm^2s^{-1} (for carbon diffusion in ferrite) and $Q = 75.6$ $KJmol^{-1}$ [27].

According to this relation, the diffusivity increases by a factor of 4.8 when the temperature is increased from 900 to 1200 ºC. In a similar manner, the diffusivity increases by a factor of 8.6 over the range from 900 to 1350 ºC. The plates formed at 900 ºC are about 200 nm or so thick [16]. Thus, the above diffusivity ratios suggest that, for equal diffusion times, the plate thicknesses at 1200 and 1350 ºC should increase to 440 and 600 nm, respectively, at these two temperatures.

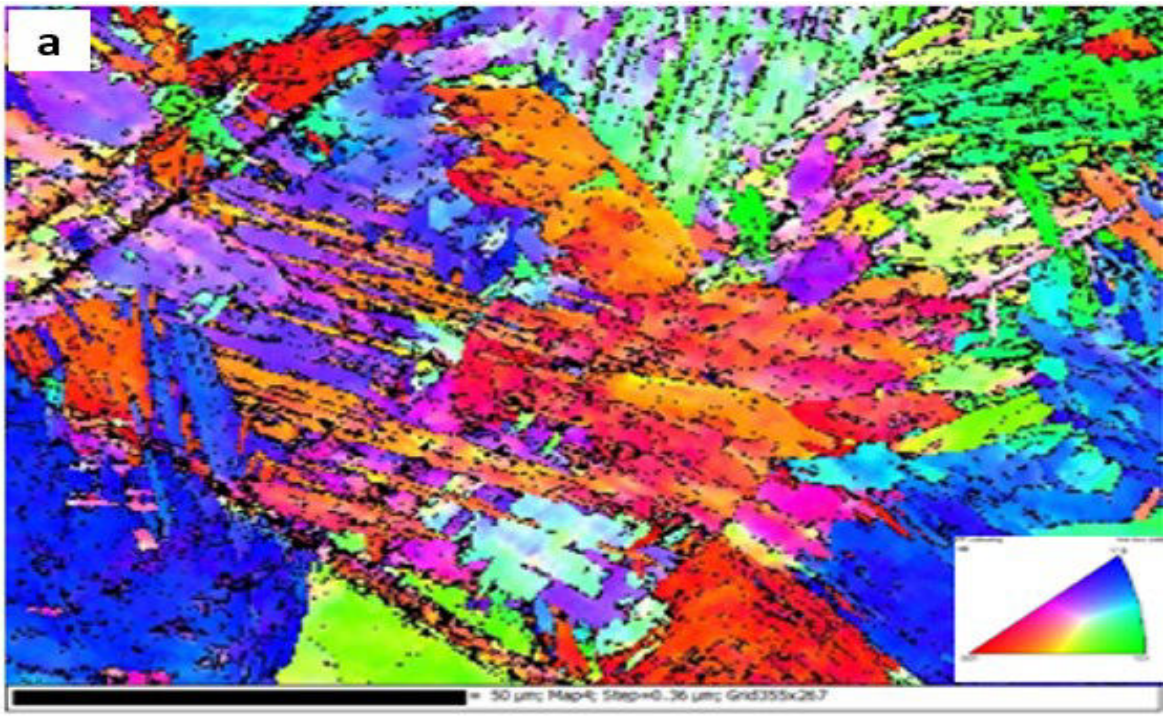

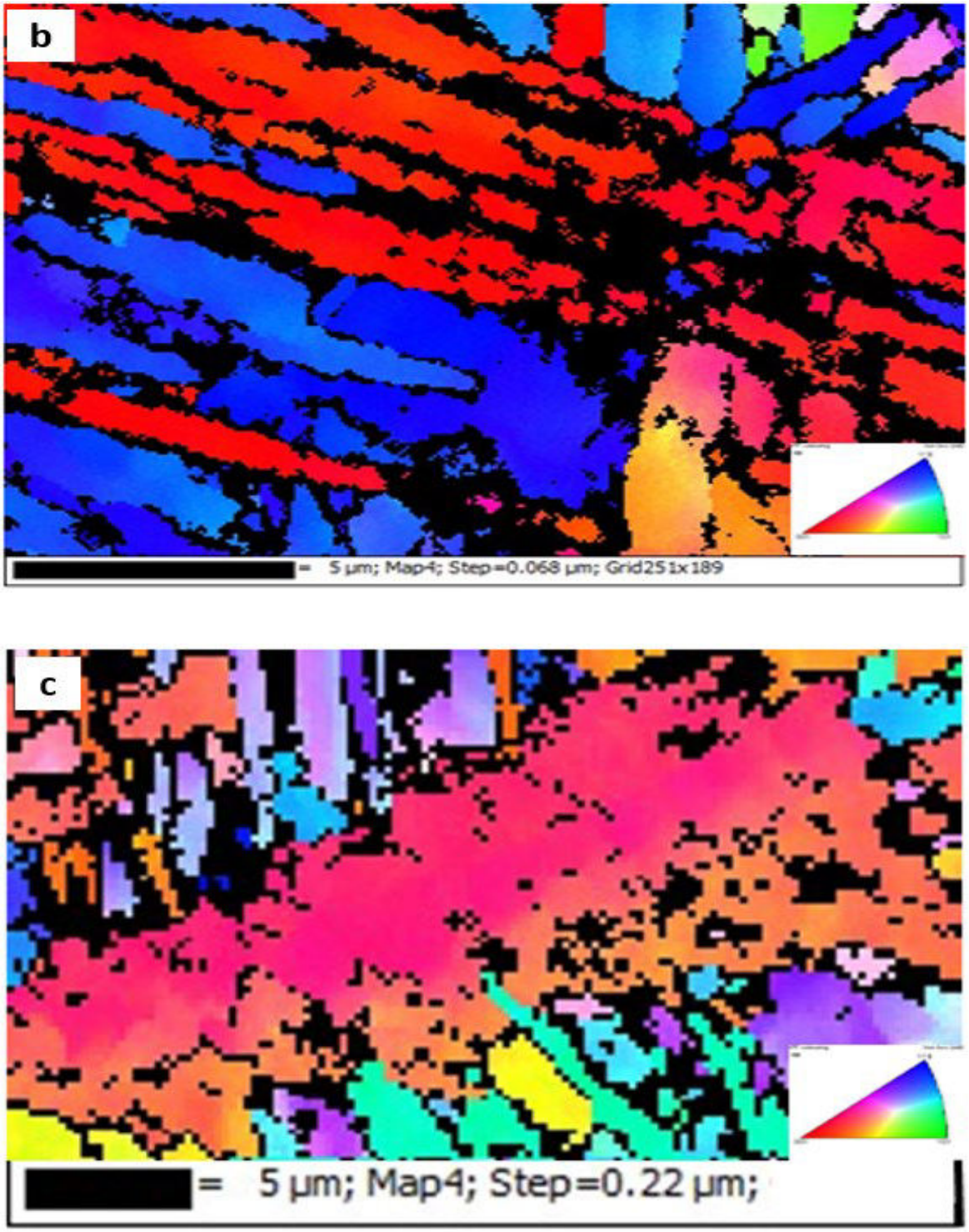

Fig. 3.10 Self-accommodating plates in sample strained to ε = 0.3 at 1200 ºC: a) 1000X, b) 7500X, c) Coalescence of plates in sample strained to ε = 0.65 at 1350 ºC and $1s^{-1}$.

Thus the increase in the rate of carbon partitioning cannot account for the full increase in plate thickness if the plate growth time is held constant. A further factor that may be playing a role is the increasing recovery rate associated with the increase in temperature. The plates form in sequences of self-accommodating pairs, the second of which is induced so as to relieve the internal stresses developed during accommodation of the first member of the pair [26]. As the rate of development of the internal stress depends on the recovery rate, larger strains and therefore times (and amounts of plate growth) are probably associated with the higher temperature tests.

3.3.5 Perpendicularity of the DT ferrite plates

When Widmanstätten ferrite plates form in the absence of an applied stress, their orientations are essentially random, that is within the limits set by the Kurdjumov-Sachs and other correspondence relations. In this way, all 24 K-S variants have an equal probability of appearing. By contrast, under dynamic transformation conditions, two habit plane/shear direction combinations are favored in each grain; those that lie closest to the plane and directions of maximum resolved shear stress [26].

Some examples of the presence of such perpendicular plates are provided in **Fig. 3.11**. Here the loading direction is vertical in the micrographs. These plates can be expected to have been aligned close to the maximum shear stress planes (inclined at 45^{o} with respect to the direction of applied stress) when they were formed.

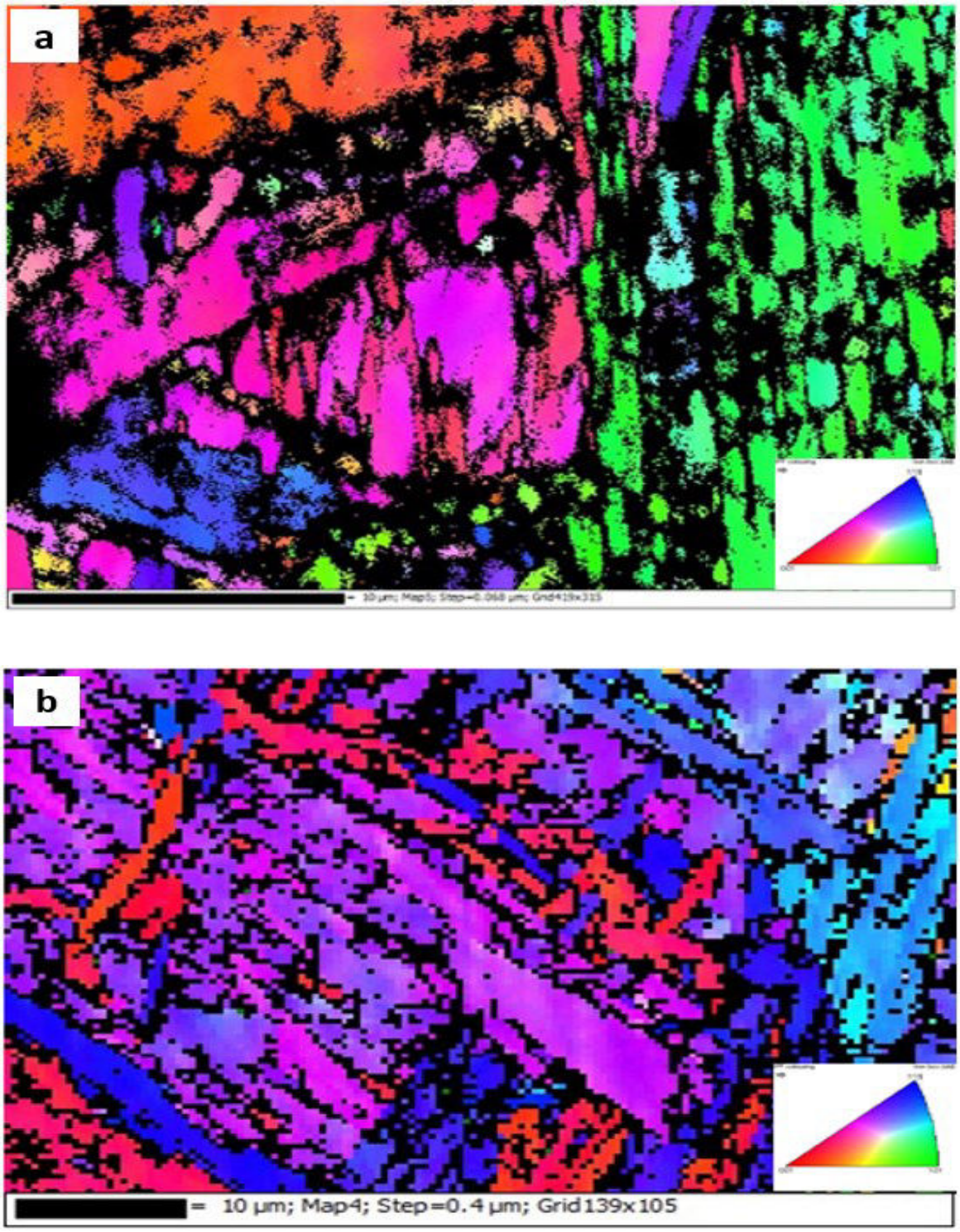

Fig. 3.11 Widmanstätten ferrite plates in samples strained to ε = 0.65 at: a) 1250 ºC and b) 1350 ºC. Note the presence of approximately perpendicular plates.

However, during compression, these plates gradually rotate away from their initial orientations by an amount that increases with the amount of strain undergone beyond the critical strain applicable to the grain in question. It can also be observed that regions with near identical orientations have coalesced into polygonal grains on further straining.

3.3.6 Plate disintegration

During these very high temperature experiments, the plates were subjected to more "break-up" than that which takes place at the lower temperatures studied to date [16-19, 28, 29]. Some examples are provided in **Fig. 3.12** illustrating the microstructures of samples strained to ε = 0.3 at 1250 and 1350 ºC. For reference, an EBSD micrograph of a sample deformed to ε = 0.3 at the somewhat lower temperature of 1200 ºC is also presented here. The rate of plate disintegration can be seen to increase with temperature. Similar trends were observed in both the low strain (0.3) and high strain (0.65) samples.

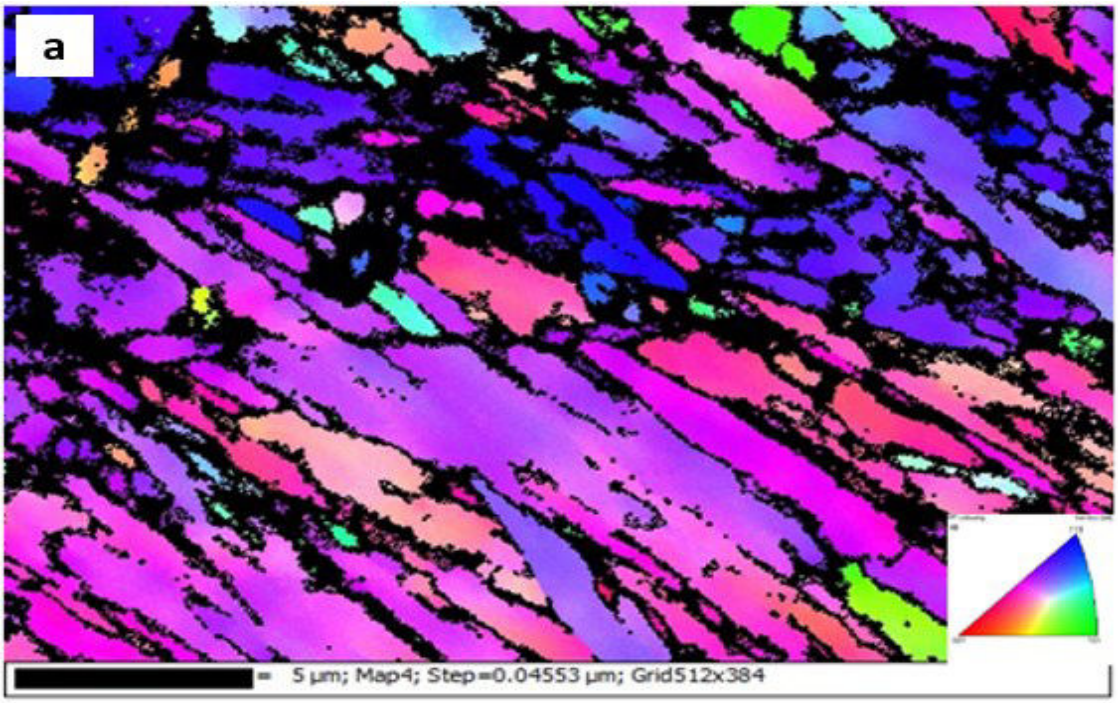

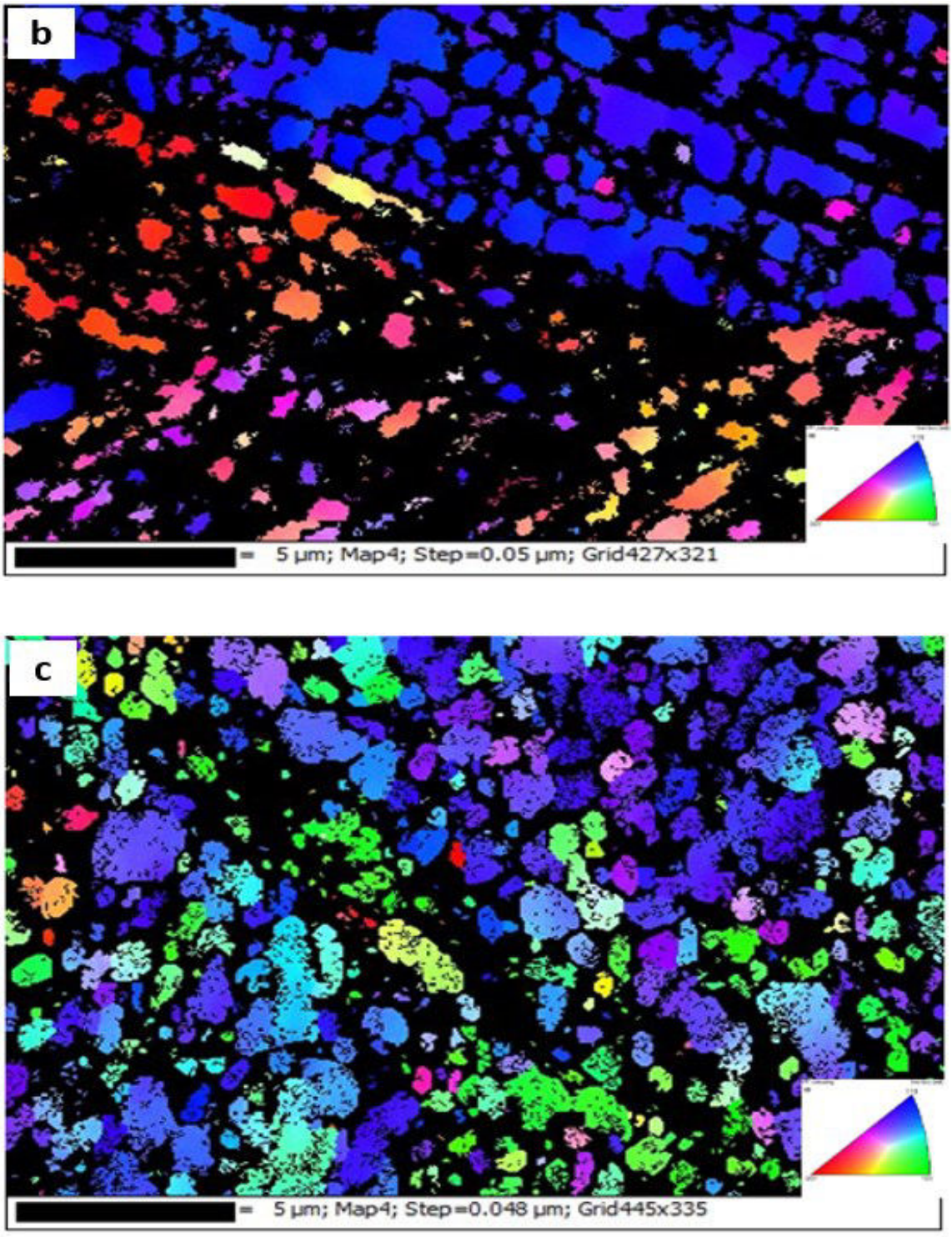

Fig. 3.12 Increasing disintegration of the ferrite plates as the temperature is increased: a) 1200 ºC b) 1250 ºC c) 1350 ºC.

3.4 Discussion

3.4.1 The Gibbs energy barrier to dynamic transformation

The observation that the critical strain for DT displays a maximum at about 1050 ºC in **Fig. 3.5 (b)** was initially surprising. So was the later finding that the volume fraction of ferrite is at a minimum at this temperature, **Fig. 3.9**. These trends can be given a physical interpretation by examining the free energy barrier to the transformation illustrated in **Fig. 3.13**. This depicts the temperature dependence of the Gibbs energy difference between the stable austenite and the metastable ferrite as a function of ΔT (experimental temperature – paraequilibrium temperature). This was calculated using the FSStel database of the FactSage thermodynamic software [20].

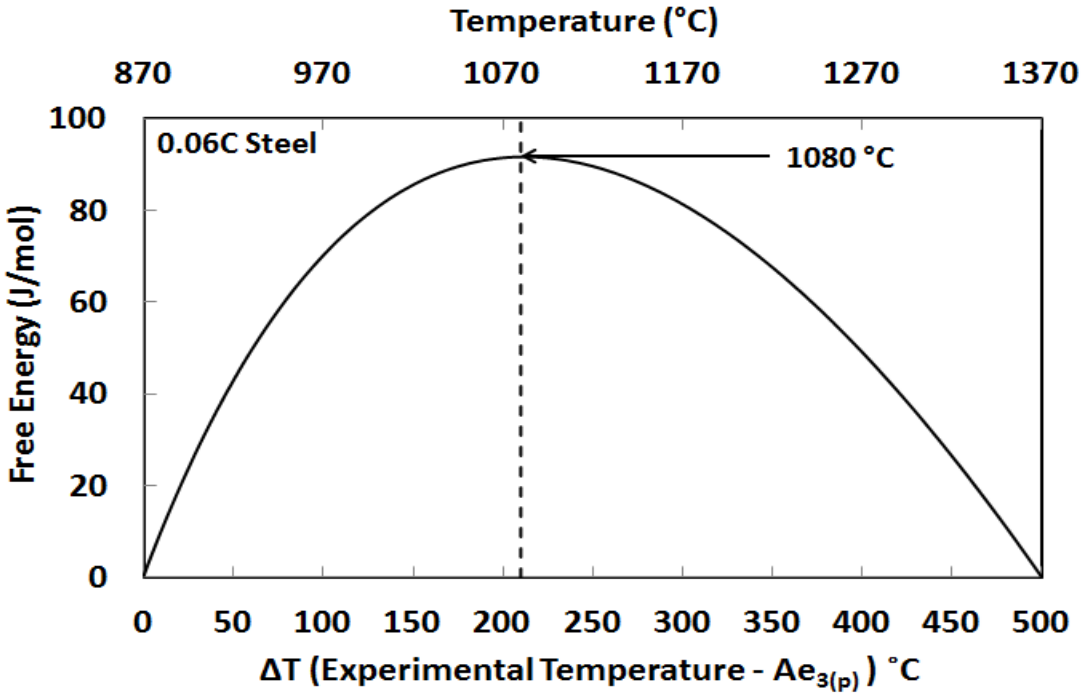

Fig. 3.13 $\Delta G_{(\gamma-\alpha)}$ vs ΔT ($Ae_{3(p)}$ – experimental temperature) for the present steel showing the Gibbs energy obstacle opposing dynamic transformation.

As can be seen, this obstacle to the transformation is at a maximum at around 1080 ºC, that is, approximately midway between the Ae_3 and the δ – ferrite phase field. This indicates that when the temperature is increased beyond the obstacle peak it becomes easier and easier to form Widmanstätten ferrite dynamically. The decrease in obstacle height in turn means that less work hardening is required in the austenite to provide the amount of transformation softening necessary to overcome the obstacle. The increasing ease of ferrite formation as the delta ferrite phase field is approached is also consistent with the ferrite volume fraction data displayed in **Fig. 3.9**.

3.4.2 A possible dynamic Fe-C phase diagram

It was shown in the previous sections that the dynamic transformation can be initiated up to 480 ºC above the paraequilibrium Ae_3 temperature. Thus the equilibrium phase diagram for undeformed material does not apply when steel is being deformed. However, the dynamic diagram depends on the amount of strain being applied and so does not have a unique configuration. An example of a possible diagram is presented in **Fig. 3.14** for an arbitrary strain. Here the Ae_3 temperature is increased by 200 to 500 ºC, depending on the carbon content. The area associated with the single austenite phase field also shrinks significantly, resulting in an increase in the area of the two-phase (α+γ) region. Moreover, the single phase ferrite region extends right up to the melting temperature.*

* See Appendix for a corrected version of **Fig. 3.14b**. This will replace the current version (p. 69) when the article is revised for publication.

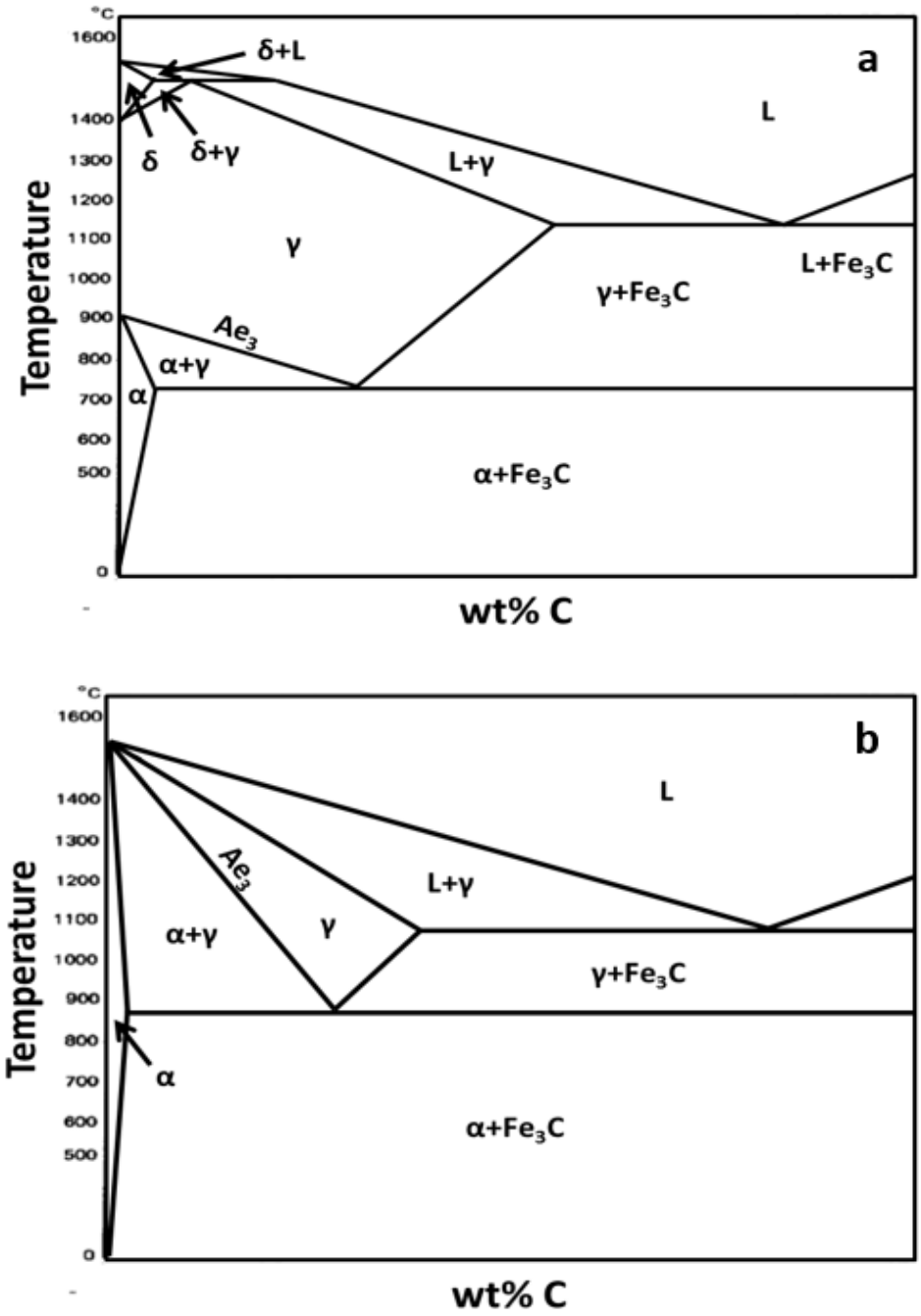

Fig. 3.14 a) Static Fe-C binary phase diagram; b) schematic dynamic (metastable) phase diagram. Note that: i) the single phase α region extends right up to the melting point; ii) the two-phase (α+γ) region is extended to much higher temperatures and; iii) the extent of the single phase γ region is reduced considerably.

3.5 Conclusions

1. The critical strains for the initiation of dynamic transformation and dynamic recrystallization were calculated using the double differentiation method. The DRX strains decreased with increasing temperatures in the conventional manner. By contrast, the critical strains for DT increased initially with temperature but then decreased as the temperatures approached the δ- ferrite phase field. This is consistent with the shape of the Gibbs energy obstacle to the transformation, which is at a maximum approximately midway between the Ae_3 and the δ- ferrite phase field.

2. Optical micrographs confirmed the presence of dynamically formed ferrite plates at temperatures as high as 1350 ºC ($Ae_{3\,(p)}$ + 480º). The ferrite volume fraction increased with the magnitude of the temperature interval above the Gibbs energy peak. This observation is also consistent with the tendencies displayed by the free energy obstacle and the DT critical strains.

3. The Widmanstätten ferrite plates produced at these very high temperatures have thicknesses of about 1 to 2 μm and are therefore about an order of magnitude wider than the plates formed at 900 ºC. This can be attributed to the higher diffusivity of carbon at these temperatures, as well as to the lower rate of work hardening. The latter is probably responsible for the somewhat slower rate of plate propagation at these very high temperatures.

4. The ferrite plates that form dynamically are frequently aligned along two approximately perpendicular directions. These correspond to the traces of planes close to the planes of maximum shear stress at the moment of plate formation. There is considerably more plate

disintegration and break-up than observed in the microstructures produced at lower temperatures.

5. The present observations indicate that the well-known ‘static’ Fe-C phase diagram does not apply when austenite is being deformed. However, the appropriate ‘dynamic’ diagram depends on the applied strain. Beyond the critical strain for the formation of Widmanstätten ferrite, the single phase α region is expanded considerably, the single phase γ region is conversely reduced in size, and the Ae_3 temperature is raised by up to 500 ºC.

Acknowledgements

The authors acknowledge with gratitude funding received from the McGill Engineering Doctoral Award (MEDA) program and the Natural Sciences and Engineering Research Council of Canada.

3.6 References

1. Y. Matsumura, H. Yada, Evolution Deformation of Ultrafine- Grained Ferrite in Hot Successive Deformation, Transactions ISIJ. 27 (1987), 492-498.
2. H. Yada, T. Matsumura, T. Senuma, Proc. Int. Conf. Physical Metallurgy of Thermomechanical Processing of Steels and Other Metals, ISIJ, THERMEC 88, (1988) 200-207.
3. H. Yada, C.M. Li, H. Yamagata, Dynamic γ→α Transformation during Hot Deformation in Iron-Nickel-Carbon Alloys, ISIJ international. 40 (2000), 200-206.
4. Y. Chen, Q. Chen, Dilatometric Investigation on Isothermal Transformation after Hot Deformation, J. Iron & Steel Res. Int. 10 (2003) 46-48.
5. H. Dong, X. Sun, Deformation Induced Ferrite Transformation in Low Carbon Steels, Current Opinion in Solid State Mater. Sci. 9 (2005) 269-276.
6. M. Tong, J. Ni, Y. Zhang, D. Li, Y. Li, Monte Carlo-Method Simulation of the Deformation-Induced Ferrite Transformation in the C-Fe system, Metallurgical and Materials Transactions A. 35A (2004) 1565-1577.
7. N. Xiao, M. Tong, Y. Lan, D. Li, Y. Li, Coupled Simulation of the Influence of Austenite-Ferrite Transformation on the Subsequent Isothermal Austenite-Ferrite Transformation, Acta Mater. 54, (2006) 1265-1278.
8. N. Park, S. Khamsuk, A. Shibata, N. Tsuji, Effect of Austenite Grain Size on Kinetics of Dynamic Ferrite Transformation in Low Carbon Steel, Scripta Mater. 68 (2013) 611-614.
9. N. Park, A. Shibata, D. Terada, N. Tsuji, Flow Stress Analysis for Determining the Critical Condition of Dynamic Ferrite Transformation in 6Ni-0.1C Steel, Acta Mater. 61 (2013) 163-173.

10. N. Park, S. Khamsuk, A. Shibata, N. Tsuji, Occurrence of Dynamic Ferrite Transformation in Low Carbon Steel Above Ae_3, Scripta Mater. 68 (2013) 538-541.
11. X. Sun, H. Luo, H. Dong, Q. Liu, Y. Weng, Microstructural Evolution and Kinetics for Post-Dynamic Transformation in a Plain Low Carbon Steel, ISIJ International. 48 (2008) 994-1000.
12. D.N. Hanlon, J. Sietsma, S. van der Zwaag, Effect of Plastic Deformation of Austenite on the Kinetics Subsequent Ferrite Formation, ISIJ International. 41 (2001) 1028-1036.
13. C. Ghosh, V.V. Basabe, J.J. Jonas, Y-M. Kim, I-H. Jung, S. Yue, The Dynamic Transformation of Deformed Austenite at Temperatures above the Ae_3, Acta Materialia. 61 (2013) 2348-2362.
14. J.J. Jonas, C. Aranas, V.V. Basabe, C. Ghosh, Dynamic Transformation during the Torsion Simulation of Strip Rolling, Materials Science Forum. 783-786 (2014) 39-44.
15. C. Ghosh, V.V. Basabe, J.J. Jonas, Thermodynamics of Dynamic Transformation of Hot Deformed Austenite in Four Steels of Increasing Carbon Content, Material Science & Engineering A. 591 (2014) 173 -182.
16. J.J. Jonas, C. Ghosh, Role of Mechanical Activation in the Dynamic Transformation of Austenite, Acta Materialia. 61 (2013) 6125-6131.
17. C. Aranas, J.J. Jonas, Dynamic Transformation of Austenite to Ferrite during the Torsion Simulation of Strip Rolling, Materials Science and Technology (MS&T) 2014 Proceedings, Pittsburgh, Pennsylvania, USA. (2014) 461-468.
18. C. Aranas, J.J. Jonas, Effect of Mn and Si on Dynamic Transformation of Austenite Above the Ae_3 Temperature, Acta Materialia. 82 (2015) 1-10.

19. C. Aranas, T. Nguyen-Minh, R. Grewal, J.J. Jonas, Flow Softening-based Formation of Widmanstätten Ferrite in a 0.06%C Steel Deformed Above the Ae_3, ISIJ International. 55 (2015) 300-307.
20. C.W. Bale, E. Belisle, P. Chartrand, S.A. Decterov, G. Eriksson, K. Hack, I.H. Jung, Y.Y. Kang, J. Melancon, A.D. Pelton, C. Robelin, S. Peterson, FactSage Thermomechanical Software and Database –Recent Developments, Calphad. 33 (2009) 295-311.
21. J.O. Andersson T. Helander, L. Hoglund, P. Shi, B. Sundman, THERMO-CALC & DICTRA, Computational Tools for Materials Science, Calphad. 26 (2002) 273-312.
22. E. Poliak, J.J. Jonas, A One-Parameter Approach to Determining the Critical Conditions for the Initiation of Dynamic Recrystallization, Acta Materialia. 72 (2014) 13-21.
23. C. Ghosh, V.V. Basabe, J.J. Jonas, Determination of the Critical Strains for the Initiation of Dynamic Transformation and Dynamic Recrystallization in For Steels of Increasing Carbon Contents, Steel Res. Int. 84 (2013) 490-494.
24. C. Aranas, S.F. Rodrigues, R. Grewal, J.J. Jonas, “Ferrite Formation Above the Ae3 Temperature during the Torsion simulation of Strip Rolling,” ISIJ International, 55 (2015) 2426-2434.
25. C.R. Brooks: Principles of the Heat Treatment of Plain Carbon and Low Alloy Steels, (1996).
26. J.J. Jonas, Y. He, G. Langelaan, “The Rotation Axes and Angles Involved in the Formation of Self-Accommodating Plates of Widmanstätten Ferrite, Acta Materialia. 72 (2014) 13-21.
27. C. Ghosh, V.V. Basabe, J.J. Jonas, Dynamic Transformation Behavior of Deformed High Carbon Steel at Temperatures Above the Ae_3, ISIJ International. 53 (2013) 900-908.

28. V.V. Basabe, J.J. Jonas, C. Ghosh, Formation of Widmanstätten Ferrite in a 0.036% Nb Low Carbon Steel at Temperatures Above the Ae_3, Steel Res Int. 85 (2013) 8-15.
29. V.V. Basabe, J.J. Jonas, The Ferrite Transformation in Hot Deformed 0.036% Nb Austenite at Temperature Above the Ae_3, ISIJ international. 50 (2010) 1185-1192.

Chapter 4: Summary

- Compression tests were carried out on a 0.06wt%C-0.3wt%Mn-0.01wt%Si steel so as to investigate the formation of Widmanstätten ferrite at very high temperatures in the austenite phase field. The experiments were performed on a Gleeble 3800 thermomechanical simulator in a vacuum environment over the temperature range 1000 to 1350 ºC at 50º intervals. Strains of 0.3 and 0.65 were employed in the tests with the strain rate held constant at 1 s^{-1}. The water quenched samples were then studied under optical and EBSD techniques.
- Optical micrographs revealed the presence of DT ferrite at temperatures as high as 1350 ºC ($Ae_{3(p)}$ + 480º). The volume fraction of ferrite increased with temperature after reaching a minimum where the obstacle to dynamic transformation is highest, that is midway between the Ae_3 and the δ-ferrite phase field. As the temperature approached the δ-ferrite region, the volume fraction of ferrite increased again. This behavior is also consistent with that of the DT critical strains.
- The EBSD micrographs showed that the Widmanstätten ferrite plates formed had thicknesses of 1 to 2 μm. These plates were an order of magnitude thicker than the plates formed below 1000 ºC. This is attributed in part to the higher diffusivity of carbon at these temperatures. The ferrite plates formed at these temperatures displayed considerably more disintegration than the plates formed at lower temperatures. Some of the plates were aligned perpendicularly. This is attributed

to the view that these plates were formed on habit planes close to the maximum shear stress planes and that on further compression, the plates rotated away from their initial orientations.

- The results of present investigation suggest that the conventional Fe-C phase diagram for undeformed material does not apply when austenite is being deformed. The appropriate dynamic or metastable phase diagram depends on the applied strain. This leads to the expansion of the single phase α-region and the α+γ region. These changes, in turn, shrink the magnitude of the single phase γ-region. The upper limit of the Ae_3 line is also moved up by about 500º.

Appendix: Correction to Fig. 3.14b

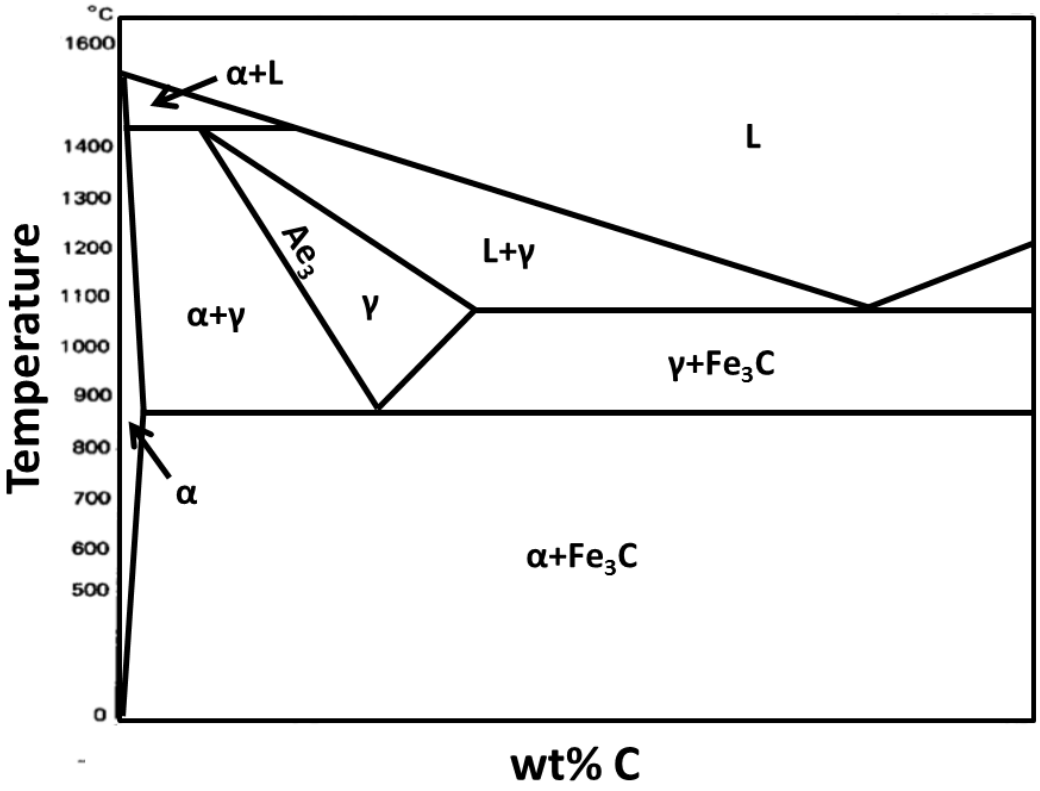

Fig. A.1 Corrected version of the schematic dynamic (metastable) phase diagram of **Fig. 3.14b**.

This schematic representation of the dynamic phase diagram showcases the peritectic region, which was not shown in **Fig. 3.14b** above. Here, the single phase γ region has shrunk, giving way to enlargement of the two-phase (α+γ) region. Concurrently, the Ae_3 temperatures have increased by 200 - 500 ºC.